Effect of CO_2/H_2S on Seamless and ERW Tubular Goods

Final Report No. 57-11162
Contract No. 23440-8-9179/01-SQ

C & M Engineering Ltd.
2220 39th Avenue N.E.
Calgary, Alberta
T2E 6P7

Attention: Mr. Colin Duncan

Submitted by:

R. W. Elliott
R. T. Lassau
Metals & Corrosion Technologies

April 30, 1991

MICROMEDIA

72 pp

ORTECH
INTERNATIONAL
2395 Speakman Drive
Mississauga, Ontario L5K 1B3
(416) 822-4111
Telefax (416) 823-1446

We, ORTECH Corporation, conducting business as "ORTECH International", stipulate that this document is subject to the following terms and conditions:
1. Any proposal contained herein was prepared for the consideration of the addressee only. Its contents may not be used by nor disclosed to any other party without our prior written consent.
2. Any testing, inspection or investigation performed by us will be conducted in accordance with normal professional standards. Neither we nor our employees shall be responsible for any loss or damage resulting directly or indirectly from any default, error or omission.
3. Any report, proposal or quotation prepared by us refers only to the particular material, instrument or other subject referred to in it. No representation is made that similar articles will be of like quality.
4. No report issued by us shall be published in whole or in part without our prior written consent.
5. Our name shall not be used in any way in connection with the sale, offer or advertisement of any article, process or service.
6. We reserve the right not to commence and/or continue any work until payment arrangements satisfactory to us are established.

ORTECH

Effect of CO_2/H_2S on Seamless and ERW Tubular Goods
For C & M Engineering Ltd.

TABLE OF CONTENTS

		Page
EXECUTIVE SUMMARY		1
1.	INTRODUCTION	5
2.	OBJECTIVES	5
3.	PROCEDURES	6
	3.1 Autoclave System	
	3.2 Experimental Procedure	
	3.3 Coupon Preparation	
	3.4 X-ray Diffraction Analysis	
	3.5 Corrosion Rates	
	3.6 Metallography	
4.	RESULTS	12
	4.1 Corrosion Rate Data for Coupons Exposed to a 150°C Brine Solution in Equilibrium with a Gas Phase of 10% CO_2, 60% H_2S and 30% N_2 at 4000 psig - Experiment 1	
	4.2 Corrosion Rate Data for Coupons Exposed to a 150°C Brine Solution in Equilibrium with a Gas Phase of 70% CO_2, 30% H_2S at 4000 psig - Experiment 2	
	4.3 Corrosion Rate Data for Coupons Exposed to a 150°C Brine Solution in Equilibrium with a Gas Phase of 20% CO_2, 20% H_2S, 60% N_2 at 4000 psig - Experiment 3	
	4.4 Corrosion Rate Data for Coupons Exposed to a 100°C Brine Solution in Equilibrium with a Gas Phase of 10% CO_2, 70% H_2S, 20% N_2 at 4000 psig - Experiment 4	
	4.5 Corrosion Rate Data for Coupons Exposed to a 100°C Brine Solution in Equilibrium with a Gas Phase of 30% CO_2, 60% H_2S, 10% N_2 at 4000 psig - Experiment 5.	

TABLE OF CONTENTS (continued)

Page

4.6 Corrosion Rate Data for Coupons Exposed to a 100°C Brine Solution in Equilibrium with a Gas Phase of 80% CO_2, 20% N_2 at 4000 psig - Experiment 6

4.7 Corrosion Rate Data for Coupons Exposed to a 150°C Brine Solution in Equilibrium with a Gas Phase of 70% CO_2, 30% H_2S at 4000 psig - Experiment 7

4.8 Corrosion Rate Data for Coupons Exposed to a 150°C Brine Solution in Equilibrium with a Gas Phase of 50% CO_2, 50% H_2S at 4000 psig and a velocity of 7.7 mps - Experiment 8.

4.9 Discussion of Corrosion Rate Data

5. DISCUSSION 16

6. SUMMARY AND CONCLUSIONS 22

7. RECOMMENDATIONS FOR FURTHER STUDY 23

REFERENCES 25

Effect of CO_2/H_2S on Seamless and ERW Tubular Goods For C & M Engineering Ltd.

EXECUTIVE SUMMARY

It is important to the oil and gas industry, from a technical and economic basis, to understand the parameters which control the corrosion processes of carbon dioxide and hydrogen sulphide on tubular goods in oil and gas reservoirs. This report describes the results of a corrosion investigation directed towards determining the corrosion rates and metallurgical effects on ERW and seamless tubular carbon steel coupons exposed to aqueous carbon dioxide/hydrogen sulphide/brine environments at 100°C and 150°C.

The results of this study and the Program I and II studies have demonstrated that, at 100°C and 150°C and 4000 psig, the following conclusions may be made.

(1) The presence of hydrogen sulphide at levels in excess of 10 mole percent of the CO_2/H_2S gas phase produces corrosion rates for carbon steels in brine solution that are noticeably higher than those produced in a CO_2/brine environment.

(2) Increasing the H_2S gas phase concentration from 10 mole percent to 50 mole percent increases corrosion rates by a factor of 2 - 3 in brine solutions where HCO_3^- and Ca^{2+} were absent. Above 50 mole percent, H_2S lower corrosion rates result.

(3) The Ca^{2+} and/or HCO_3^- ions are potentially involved in reducing corrosion in H_2O/CO_2 brine solutions.

(4) Corrosion of carbon steels in CO_2/H_2S/brine solutions saturated with H_2S is a result of oxidation of the metal by H_2S; CO_2 may not

contribute significantly to the corrosion process through direct participation.

(5) Increases in CO_2 gas phase concentration above 50% accelerate corrosion in the absence of H_2S in HCO_3^- and Ca^{2+} free brine.

(6) A velocity of 7.7 mps (metres per second) accelerates corrosion slightly at 50 moles percent H_2S and CO_2 at 150°C in brine solutions.

(7) The corrosion rates of the seamless and welded grades of steel, submitted for study in this program, were similar. This implies that differences between the materials due to chemistry, heat treatment and the inclusion of welds were not significant to distinguish them by their corrosion behaviour under the experimental conditions in this study. General corrosion was the main type of corrosion observed. Some minor pitting corrosion also occurred. No significant weld-zone corrosion was observed.

SOMMAIRE EXÉCUTIF

Comprendre les paramètres contrôlant les procédés de corrosion du gaz carbonique et du sulfure d'hydrogène sur les produits tubulaires dans les réservoirs d'huile et de gaz demeure un défi d'importance primordiale pour l'industrie pétrolifère et ce, des points vue technique et économique. Ce rapport décrit les résultats d'une recherche sur la corrosion relativement à la détermination des taux de corrosion et des effets métallurgiques sur les coupons en acier tubulaire ERW et sans couture exposés aux environnements aqueux de gaz carbonique/sulfure d'hydrogène/eau salée à 100°C et 150°C.

Les résultats de cette étude et les études du Programme I et II ont démontré que, à 100°C et 150°C et à 4000 psig, les conclusions suivantes peuvent être tirées:

(1) La présence du sulfure d'hydrogène aux niveaux surpassant 10 moles pour cent de la phase gazeuse du CO_2/H_2S produit des taux de corrosion pour l'acier de carbone dans une solution d'eau salée qui sont beaucoup plus élevés que ceux produits dans un environnement de CO_2/eau salée.

(2) Le fait d'augmenter la concentration de la phase gazeuse de H_2S de 10 moles pour cent à 50 moles pour cent augmente les taux de corrosion d'un indice de 2 à 3 dans les solutions d'eau salée où HCO_3 et Ca^{2+} étaient absents. Au-dessus de 50 moles pour cent, on remarque des taux de corrosion de H_2S réduits.

(3) Les ions de Ca^{2+} et/ou HCO_3^- sont potentiellement impliqués dans la réduction de la corrosion dans les solutions d'eau salée de H_2O/CO_2.

(4) La corrosion des aciers de carbone dans les solutions d'eau salée de CO_2/H_2S saturées de H_2S s'avère le résultat de l'oxydation du métal par H_2S; le CO_2 peut ne pas contribuer de façon importante par participation directe au procédé de corrosion.

(5) Des augmentations de la concentration de la phase gazeuse du CO_2 au-dessus de 50 % accélèrent la corrosion en l'absence de H_2S dans l'eau salée sans HCO_3^- ni Ca^{2+}.

(6) Une vélocité de 7,7 mps (mètres par seconde) accélère légèrement la corrosion à 50 moles pour cent de H_2S et CO_2 à 150°C dans les solutions d'eau salée.

(7) Les taux de corrosion pour les aciers sans couture et aciers soudés soumis à l'étude dans ce programme étaient similaires. Par conséquent, on considère que les différences entre les matériaux attribuables à la chimie, au traitement de chaleur et à l'inclusion de soudures n'étaient pas assez importantes pour les distinguer quant à leurs caractéristiques de corrosion dans les conditions expérimentales utilisées dans cette étude. La corrosion générale a été le principal type de corrosion observé. Une légère corrosion par piqûre a également été observée. Aucune corrosion importante de la zone de soudure n'a été observée.

1. INTRODUCTION

The corrosion of materials under the influence of carbon dioxide and hydrogen sulphide is of great interest to the oil and gas industry. Either one cr both of these gases are naturally occurring in oil and gas reservoirs. In addition, enhanced oil recovery methods such as steam stimulation and in situ combustion expose downhole tubular materials to significant levels of produced hydrogen sulphide and carbon dioxide at temperatures well in excess of the natural reservoir temperature. This results in excessive corrosion in both injection and production wells and surface facilities. A possible extension of the useful life of downhole tubular materials, if only by 50 percent, would achieve considerable reduction in capital and operating costs. Thus, it is important from a technical and economic basis, to understand the parameters which control the corrosion processes of carbon dioxide and hydrogen sulphide on tubular goods.

This report describes the results of a corrosion investigation directed towards determining the corrosion rates and metallurgical effects of tubular carbon steel coupons exposed to aqueous carbon dioxide/hydrogen sulphide/brine environments in the 100°C - 150°C range at a total pressure of 4000 psig (27.58 mPa).

2. OBJECTIVES

The objectives of the program were to characterize and elucidate the mechanism of corrosion damage affecting the performance of both ERW and seamless tubular goods exposed to CO_2/H_2S brines at 100°C and 150°C. In particular, the effect of adding H_2S gas to a CO_2/brine solution, on the corrosion of seamless and ERW carbon steel

coupons was determined by comparing the results of this program to those of the Program I study (Report No. 57-10486, Contract No. 035Q-233440-5-9032, Effect of CO_2 on Seamless and ERW Tubular Goods, January 27, 1987), and the Program II study (Report No. 57-10731, Contract No. 03SQ-23440-5-9032, Effect of CO_2/H_2S on Seamless and ERW Tubular Goods, April 30, 1988). Two additional objectives were to: (1) seek further confirmation of corrosion inhibition by sodium bicarbonate and calcium chloride of seamless and ERW goods in H_2S/CO_2/brine solutions and (2) determine if velocity has an effect on corrosion of seamless and ERW goods in H_2S/CO_2/brine solutions.

3. PROCEDURES

3.1 Autoclave System

All experiments were conducted in a 2-gallon Hastelloy C autoclave. The autoclave was equipped with gas and liquid sampling ports, a gas injection line and magnetic stirring to provide solution agitation. The autoclave was heated by a 3-zone heater that provided temperature control to ±2°C of the set point. The autoclave has maximum operating pressure and temperature limits of 5000 psi (34.47 mPa) and 500°C, respectively. Figure 1 is a schematic drawing of the autoclave used in the experiments.

3.2 Experimental Procedure

For the purpose of the corrosion experiments, three (3) coupons of each steel grade were mounted on a Teflon coupon tree. The chemical composition of each steel grade is listed in Table I. Each

coupon was suspended on stainless steel wire that was coated with Teflon™ tubing. This ensured that each coupon did not contact any dissimilar metal surfaces. Experiments were conducted in a solution identical to that of ASTM D 1141 except that $NaHCO_3$ and $CaCl_2$ were replaced by an equivalent number of moles of NaCl. One experiment was conducted in unmodified ASTM D 1141 brine. Table II lists the concentrations of the various brine solution components.

The baffle was removed from the autoclave for the velocity experiment. Two Teflon™ rectangular blocks were drilled and equipped with two set screws to hold them on the shaft. A hole was drilled and tapped in each end of the Teflon™ blocks. Two coupons which had a hole drilled and countersunk in their centre were mounted to each block with Teflon™ screws. The leading edge of each Teflon™ block was tapered to minimize drag. The thermocouple well in the autoclave limited the maximum coupon surface-to-surface spacing to $3^{5}/_{16}$ inches. The highest stable rotation speed that the stirrer was able to maintain was 1750 rpm which resulted in a velocity of 7.7 metres per second (25.3 feet per second). One seamless (S0095) coupon and one ERW (ILW80) coupon were exposed in duplicate in ASTM D 1141 brine.

Sufficient brine was used to cover all coupons with the aqueous phase during the experiments, such that the volume/area ratio was greater than 10 ml/cm^2. It is important to note that the brine was boiled for one half hour prior to each experiment to minimize dissolved oxygen levels. Care was taken to ensure that evaporative losses did not occur, and therefore the concentration of HCO_3^{-1} was not altered during this procedure. After boiling, nitrogen gas was bubbled through the brine solution to complete oxygen removal and to prevent the reabsorption of oxygen.

A total of eight (8) autoclave experiments were conducted and the specific conditions of each experiment are summarized in Table III. All experiments were terminated after 14 days.

The procedure used for each experiment is described in the following sequence of events. The coupons and deoxygenated brine were placed in the autoclave which was then sealed. The oxygen, in the air space above the liquid brine, was removed by evacuating the autoclave and repressurizing the system with oxygen free nitrogen to a total pressure of 500 psig. The autoclave was then heated to the required temperature, while the solution was stirred vigorously to achieve equilibrium. A compressor was used to achieve the required gas mixture in the autoclave. The total operating pressure for each experiment was 4000 psig.

Gas chromatography was used in each test to ensure that the gas phase concentrations of carbon-dioxide and hydrogen sulphide were ±5 volume percent of the required levels. Dissolved oxygen was determined using a dissolved oxygen test kit (Chemetrics Inc.), and was found to be less than 0.1 ppm for all experiments, except experiment No. 6. The oxygen concentration in that experiment is estimated at 1 ppm (see discussion).

3.3 Coupon Preparation

The ERW and seamless carbon steel coupons were received by ORTECH International from C & M Engineering of Calgary. The ERW material was originally provided by IPSCO (Regina, Saskatchewan) and consisted of steel grades IJW55, IKW55 and IL80. The seamless material was provided by Algoma Steel (Sault Ste. Marie, Ontario) and

consisted of steel grades K55, L80 and S0095. The chemical composition of the test materials is listed in Table I. ORTECH received a total of 271 numbered coupons prepared by C & M Engineering. All coupons were prepared by cutting them to uniform dimensions and providing uniform surface and edge finishes.

The coupons had approximate dimensions of 1.5 cm x 3.5 cm x 0.3 cm. The IJW55 samples were derived from 5 1/2" O.D. (13.97 cm) and 0.275" (0.70 cm) wall thickness ERW casing. The IJW55 is a medium carbon, low sulphur steel in a full body normalized condition. The IKW55 samples were derived from 7" O.D. (17.78 cm) and 0.272" (0.69 cm) wall thickness ERW casing. The IKW55 is a medium carbon, low sulphur steel microalloyed with molybdenum and vanadium, in a full body normalized condition. The IL80 samples were derived from 7" O.D. (17.78 cm) and 0.362" (0.92 cm) wall thickness ERW casing. The IL80 is a medium carbon, low sulphur steel microalloyed with vanadium and molybdenum, in quenched and tempered condition. The Algoma Steel samples were derived from 9.5" O.D. (24.13 cm) casing. Algoma K55 was supplied in a normalized condition. Algoma L80 and S0095 are specialty grades for H_2S services, and were supplied in a quenched and tempered condition.

Coupon surfaces were finished using a glass bead technique, except for a duplicate set of coupons of one seamless and one ERW material which were polished to 320 grit and included in Experiment 1.

For the purpose of determining corrosion rates using weight loss measurements, the coupons were degreased in acetone, weighed and dimensioned to determine surface areas. All coupons were stored in a desiccator until required for a particular experiment. This eliminated any potential corrosion of the carbon steel surfaces by humid air.

3.4 X-ray Diffraction Analysis

X-ray diffraction analyses were conducted using a Philips recording diffractometer to identify crystalline phases present in the corrosion products. The filmed surface of one coupon removed from each experiment was used for these analyses. Note, the scope of the program was not sufficient for X-ray analyses to be conducted on all steel types exposed to each of the chemical environments. All X-ray spectra were carefully examined to ensure that all chemical compounds (i.e. metal oxides, metal hydroxides, metal sulphides, metal carbides, and metal carbonates) were detected. Table IV summarizes the results of the X-ray diffraction analysis.

3.5 Corrosion Rates

The corrosion rates were calculated from weight loss data. The measured weight loss and the calculated corrosion rates are presented in Tables V to X.

Corrosion rates were calculated from weight loss data using the following equation:

$$\text{Corrosion rate } \frac{mm}{yr} = \frac{87.6\ W}{DAt}$$

87.6	=	constant to provide corrosion rates in mm/yr.
W	=	weight loss in milligrams
D	=	density in g/cm^3 (taken as 7.86 g/cm^3 for all steel grades)
A	=	coupon area in cm^2
t	=	experimental time in hours.

The corrosion product on the coupons was removed by first cleaning them in a mild detergent, followed by exposure to Clark's solution (concentrated hydrochloric acid, inhibited with stannous chloride and antimony trioxide). The acid cleaning was continued until most, if not all, of the product had been removed. This was determined by examining the coupon surface with an optical microscope and, where necessary, continuing the cleaning process until all the coupon surface was judged to be free of corrosion products. Weight loss due to the acid cleaning was determined to correspond to a corrosion rate of approximately 0.03 mm/year.

3.6 Metallography

Six different steel products were investigated in this corrosion study. The different grades of steels were K55, L80 and S0095 from the Algoma Steel Company and K55, J55, L80 from the IPSCO Steel Company. The materials provided by IPSCO contained an ERW seam through the centre of each coupon. The chemical compositions of the above materials are listed in Table I.

Among the Algoma Steels, the K55 has a pearlitic microstructure, while the L80 and S0095 are low alloy steels with quenched and tempered martensitic microstructures. In the case of IPSCO materials, both the IJW55 and IKW55 have fine pearlitic microstructures, whereas the ILW80 shows a quenched and tempered martensitic microstructure.

Metallographic examinations were performed on representative test coupons subjected to the corrosive environments listed in Table III, runs 1 and 2. The exposed coupons were initially examined for general

surface features, followed by a detailed metallographic examination on their cross-sections in both polished and etched conditions.
The observations made on the test coupons that were subjected to the different test environments are listed in Appendix I.

4. RESULTS

4.1 Corrosion Rate Data for Coupons Exposed to a 150°C Brine Solution in Equilibrium with a Gas Phase of 10% CO_2, 60% H_2S and 30% N_2 at 4000 psig - Experiment 1

Experiment number 1 consisted of exposing the steel coupons to a modified ASTM D 1141 brine solution (free of $NaHCO_3$ and $CaCl_2$) in equilibrium with a gas phase as noted above, for a period of 14 days. Corrosion rate data at 0.5 mm/yr. on average, are similar among all steel grades. One IKW55 coupon had a corrosion rate of 1.6 mm/year. The materials have good corrosion resistance in this test environment. The major corrosion product was troilite, FeS. Approximately 1 - 2% of the deposit was unidentified.

This run included L80 and ILW80 materials with their surfaces polished to 320 grit rather than glass beaded to compare the effects of surface preparation. The corrosion rates of these polished materials averaged 0.7 mm/year. This higher corrosion rate for polished surfaces is likely due to increased cold work. The glass beaded surface does not produce as much surface disturbance as does grit blasting which was used by de Waard and Milliams in their polarization study [1]. The grit blasted metal losses (de Waard and Milliams) were as much as 30% higher, due to corrosion, than were the polished sample metal losses.

This run included L80 and S0095 materials exposed in the vapour zone. The corrosion rates of the L80 material averaged 0.7 mm/yr. and that of two of the S0095 materials averaged 0.9 mm/yr. One of the S0095 materials exhibited a corrosion rate of 2.8 mm/yr.

4.2 Corrosion Rate Data for Coupons Exposed to a 150°C Brine Solution in Equilibrium with a Gas Phase of 70% CO_2, 30% H_2S at 4000 psig - Experiment 2

Experiment number 2 consisted of exposing the test coupons to a modified ASTM D 1141 brine solution (free of $NaHCO_3$ and $CaCl_2$) with a gas phase composition as noted above. The experiment was conducted for a 14-day period. Some difficulty was experienced with the heating elements during the latter part of this run. Consequently, approximately two days (10 and 11) were spent at less than the nominal 150°C. Therefore, corrosion rates in this experiment may be expected to be moderately low because of the lower rate of diffusion of iron to the surface of the film at lower temperatures. The predominantly pyrrhotite film grows by outward migration of iron. The corrosion rates for all materials averaged 0.5 - 0.6 mm/year with the L80 and S0095 materials exposed in the vapour phase having corrosion rates at the lower end of the range. X-ray diffraction analysis of the precipitate filtered from the brine showed the major components to be pyrrhotite (Fe_7S_8). Approximately 5 - 10% of the precipitate was marcasite (FeS_2) and 1 - 2% was sulphur (S). Approximately 2 - 5% of the precipitate was unidentified.

4.3 Corrosion Rate Data for Coupons Exposed to a 150°C Brine Solution in Equilibrium with a Gas Phase of 20% CO_2, 20% H_2S, 60% N_2 at 4000 psig - Experiment 3

Experiment 3 involved exposing the test coupons to a modified ASTM D 1141 brine solution (free of $NaHCO_3$ and $CaCl_2$), in a gas phase composition as noted above, for a period of 14 days. The corrosion rates of the immersed materials in this environment were between 0.6 and 0.7 mm/yr., except for one of the K55 coupons which had a corrosion rate of 1.6 mm/yr., while the other two coupons averaged 0.7 mm/yr. The S0095 material in the vapour zone averaged 1.0 mm/yr. The major product of corrosion in the brine was a different form of pyrrhotite, $Fe_{1-\chi}S$, than formed in Experiment 2 (Fe_7S_8).

4.4 Corrosion Rate Data for Coupons Exposed to a 100°C Brine Solution in Equilibrium with a Gas Phase of 10% CO_2, 70% H_2S, 20% N_2 at 4000 psig - Experiment 4

Experiment 4 consisted of exposing test coupons to a modified ASTM D 1141 brine solution (free of $NaHCO_3$ and $CaCl_2$), in a gas phase composition as noted above, for a period of 14 days.

The materials all exhibited corrosion rates between 0.1 and 0.6 mm/yr. The major corrosion product was pyrrhotite, $Fe_{1-\chi}S$.

4.5 Corrosion Rate Data for Coupons Exposed to a 100°C Brine Solution in Equilibrium with a Gas Phase of 30% CO_2, 60% H_2S, 10% N_2 at 4000 psig - Experiment 5

Experiment 5 consisted of exposing test coupons to a modified ASTM D 1141 brine solution (free of $NaHCO_3$ and $CaCl_2$), in a gas phase composition as noted above, for a period of 14 days. The corrosion rates are similar for all materials and average 0.2 - 0.4 mm/year. X-ray diffraction analysis of the film on one coupon showed pyrrhotite (Fe_7S_8) to be the major phase with 2 - 5% sulphur (S) and 2 - 5% unidentified.

4.6 Corrosion Rate Data for Coupons Exposed to a 100°C Brine Solution in Equilibrium with a Gas Phase of 80% CO_2, 20% N_2 at 4000 psig - Experiment 6.

Experiment 6 consisted of exposing test coupons to a modified ASTM D 1141 brine solution (free of $NaHCO_3$ and $CaCl_2$), in a gas phase composition as noted above, for 14 days. The corrosion rates averaged 1.1 to 2.4 mm/year. The corrosion products were 100% siderite, $FeCO_3$. The deaeration procedure, prior to this experiment, was not applied for as long a period of time as in subsequent experiments. The oxygen concentration is expected to have been approximately 1 ppm.

4.7 Corrosion Rate Data for Coupons Exposed to a 150°C Brine Solution in Equilibrium with a Gas Phase of 70% CO_2, 30% H_2S at 4000 psig - Experiment 7.

Experiment 7 consisted of exposing test coupons to ASTM D 1141 brine solution, in a gas phase composition as noted above, for 14 days. The corrosion rates averaged 0.6 - 0.8 mm/year with the L80 and

S0095 materials in the vapour phase having corrosion rates at the lower end of the range. X-ray diffraction analysis of the corrosion products showed the major phase to be pyrrhotite (Fe_7S_8) with 1 - 2% marcasite (FeS_2), 1 - 2% sulphur (S) and 2 - 5% unidentified components.

4.8 Corrosion Rate Data for Coupons Exposed to a 150°C Brine Solution in Equilibrium with a Gas Phase of 50% CO_2, 50% H_2S at 4000 psig and a velocity of 7.7 mps - Experiment 8.

Experiment 8 consisted of exposing test coupons to an ASTM D 1141 solution (free of $NaHCO_3$ and $CaCl_2$). in a gas phase composition as noted above, for 14 days. The coupons were rotated so that their outer surfaces experienced a velocity of 7.7 mps. The corrosion rates of the S0095 and ILW-80 materials exposed averaged 0.4 - 0.5 mm/year. X-ray diffraction analysis of the corrosion products showed the major phase to be pyrrhotite ($Fe_{1-x}S$), with pyrite (FeS_2) 10 - 20%, marcasite (FeS_2) 5 - 10% and unidentified materials 1 - 2%.

5. DISCUSSION

All coupons were covered with a black solid film after exposure to their respective environments. Table IV is a summary of the corrosion products found on coupons after each experiment. The X-ray diffraction data clearly indicate that the major corrosion product from each experiment involving H_2S was pyrrhotite or troilite. Metal carbonates such as $FeCO_3$ were not detected, except in the H_2S free experiment. Hydrogen sulphide is largely responsible for corrosion of the carbon steel coupons. The corrosion process may be represented by the following reactions:

$H_2S + (1-\chi)\ Fe \rightarrow Fe_{1-\chi}S + H_2 \uparrow$, or
$H_2S + Fe \rightarrow FeS + H_2 \uparrow$.
$2H_2S + Fe \rightarrow FeS_2 + 2H_2 \uparrow$

The corrosion rate data are presented in Tables V to X, and Table XI provides an average corrosion rate and 90% confidence limit from the t distribution. Table XII lists the average corrosion rates for all three programs (Report No. 57-10486, dated January 27, 1987 and Report No. 57-10731, dated April 30, 1988) separated as to temperature (100°C or 150°C) and brine (D 1141 or modified D 1141). Figure 2 presents the data of Table XII graphically as a function of CO_2 and H_2S additions. Upon examination of the data, the following conclusions can be drawn:

(1) for any experiment, the corrosion rates for the seamless and ERW materials are similar. This indicates that the differences in chemical composition, and structural features, including the welded seam, between the materials, has a minimal influence on the corrosion rates in H_2S/CO_2 brine solutions;

(2) comparison of the corrosion rate data for those experiments which involved the use of the ASTM D 1141 brine with $NaHCO_3$ and $CaCl_2$ replaced by an equivalent number of moles of NaCl, indicates that increasing the H_2S gas phase concentration to about 50% results in a substantial increase in corrosion rates for all steel types. This again emphasized the fact that the steel grades or types of steel cannot be selectively differentiated in these environments.

Comparison of the corrosion rates of this study with those of the CO_2/H_2S Program II and the CO_2 Program I study (Table XII and Figures 2 and 3) clearly suggest that the presence of hydrogen

sulphide increases the extent of corrosion of the test materials up to 50% H_2S. The results of the Program I study indicated that passivation of the coupon surfaces was occurring due to the formation of a hard non-permeable siderite film. The film formed in the presence of H_2S consisted mostly of two forms of pyrrhotite $Fe_{1-\chi}S$, or Fe_7S_8, and does not passivate the coupon surfaces to the same degree as siderite. Formation of troilite, FeS which occurred in Experiment 1 (150°C, 60% H_2S, 10% CO_2) may provide some inhibitive effect. Marcasite or pyrite (FeS_2), which formed in some experiments, may have a similar effect. The pyrrhotite grows by migration of Fe to the surface. B. R. D. Gerus [2] suggests that the more perfect crystal structure of pyrite and troilite reduces cation diffusion to a minimum. He also reports that the pH of the water, which could be influenced by the CO_2 partial pressure, also appears to influence the iron sulphide formed.

A small amount of elemental sulphur was detected in the corrosion products from Experiments 2, 5 and 7. Sulphur could form as a result of air oxidation of water wet samples, however this sulphur is expected to be amorphous and would not be detectable by X-ray diffraction. In addition, the coupons were rinsed with water immediately after removal from the autoclave and then with acetone, and air dried. Since the coupons were still well above ambient temperature, they dried quickly. Formation of elemental crystalline sulphur could have a considerable effect on the corrosion of these materials.

The nature of the corrosion products: (1) different forms of pyrrhotite, (2) the formation of stoichiometric troilite and marcasite and (3) the formation of small amounts of elemental sulphur, merit further study so that their effect on the corrosion rates can be determined.

The results of the earlier Program II and the Program III studies show that hydrogen sulphide, not carbon dioxide, is more aggressive toward steel surfaces. This was determined by analysis of the corrosion products on the filmed surfaces. It is reasonable to conclude then that as H_2S levels are increased in CO_2/brine solutions, the H_2S eventually becomes the major influence on the corrosion of carbon steel surfaces.

As can be seen from the composition of deposits on the coupons, Table IV, any addition of H_2S to the CO_2 containing reactor environment makeup produces iron-sulphur in preference to iron-carbonate compounds. This evidence in itself is sufficient to demonstrate that H_2S plays the dominant corrosion role in the mixture. In addition, adding H_2S to environments with constant CO_2 concentrations produces an "apparent" straight line relationship (Figure 3; Δ, 50% CO_2), suggesting that the corrosion rate, under the conditions studied, is first order in $[H_2S]$

Is there a family of curves that can be generated? Given a common origin for 0% H_2S additions of between 0.1 and 0.2 mm/yr. (Figure 3), lines can be drawn (assuming linearity) connecting points of constant CO_2 concentration. With two exceptions, the data show that as the initial CO_2 construction is increased so is the slope of the "curve" resulting from connecting corrosion rate/H_2S addition points. The exceptions are noted to be at constant CO_2 concentrations of 20% and 70% (Δ points).

There is, therefore, evidence suggesting that a family of curves exists depicting the corrosion rates of OCTG (Oil Country Tubular Goods) materials in brines containing CO_2 to which H_2S is added.

Oxygen removal in the 80% CO_2, 20% N_2 run, Experiment 6, was not as complete as in the other five and it is suspected that the oxygen concentration was ~1 ppm. No iron oxides were detected in the corrosion products which would be expected if oxygen played a serious accelerating role. Therefore, it appears that acceleration of the corrosion occurs at >50% CO_2 concentration in the absence of H_2S at 150°C. Because siderite is protective, the majority of the corrosion would occur early in the exposure. The duration of the Program I work was 28 days and that of this work was 14 days. The corrosion rate in the shorter duration test would then appear to be higher.

Some difficulty was experienced with the stirrer in some experiments in that the coupon rack apparently shifted, causing the impeller shaft to occasionally rub against one or two coupons, resulting in mechanical damage. Mechanically damaged coupons were excluded from average corrosion rate calculations. The depressions (see Figure 7 in the Appendix) which formed in some of the coupons may be the result of galvanic corrosion and/or crevice corrosion between the scale and parent metal. This form of attack appeared at the higher temperature. In several experiments one of the three coupons showed a much higher or much lower corrosion rate than the other two. In each case, the coupons with the higher corrosion rate had a greater weight of adherent corrosion products. This may be caused by variation in condensation in the vapour phase, splashing of brine onto coupons in the vapour phase or variations in the agitation of the brine at immersed coupon surfaces caused by differences in orientation in the brine.

Corrosion rates in the vapour phase tend to be higher than in the liquid phase at 150°C and less than in the liquid phase at 100°C. There does not appear to be any correlation with gas concentration.

Some coupons with a mottled appearance and with depressions were qualitatively alike, and differed only in the size of the features. These similarities occurred in Experiments 1 and 2 but not in Experiment 3 which was also performed at 150°C. These surface features are likely related to sulphide scale formation and rupture with galvanic and/or crevice corrosion occurring under the scale. The H_2S concentration for Experiment 1 was 60%, and it was 30% for Experiment 2. Experiment 3 had only 20% H_2S.

Velocity, as applied in these experiments, does not appear to accelerate corrosion of the coupons appreciably. The corrosion products formed in Experiment 8, included a much higher concentration of FeS_2 than found in the other experiments.

The corrosion rates generated at 100°C (Experiments numbered 4 and 5) are lower than those generated at 150°C (Experiment number 1).

The data obtained in the three programs are insufficient for detailed statistical analysis because of the number of variables, all of which affect the corrosion rate. These variables, in apparent order of importance are: (1) temperature, (2) H_2S concentration, (3) CO_2 concentration and (4) brine composition. Velocity may also be a variable, but more experiments need to be performed to establish the statistics.
The metallographic observations can be found in Appendix I.

6. SUMMARY AND CONCLUSIONS

The results of this study and the Programs I and II studies have demonstrated that, at temperatures of 100°C and 150°C, the following conclusion may be made.

(1) The presence of hydrogen sulphide at levels in excess of 10 mole percent in a CO_2/H_2S gas phase produces corrosion rates for carbon steels in brine solution that are noticeably higher than those produced in a CO_2/brine environment.

(2) Increases in H_2S gas phase concentrations from 10 mole percent to 50 mole percent increase corrosion rates by a factor of 2 - 3 in brine solutions where HCO_3^- and Ca^{2+} were absent, above 50 mole percent the iron sulphide scale formed seems to become more inhibitive and lower corrosion rates result. The lower corrosion rates at the higher H_2S concentrations may be the result of a change in the type of film formed.

(3) The added HCO_3^- and Ca^{2+} ions appear to influence corrosion by reducing it in H_2S/CO_2 brine solutions.

(4) Corrosion of carbon steels in CO_2/H_2S/brine solutions saturated with H_2S is a result of oxidation of the metal by H_2S; CO_2 may not contribute significantly to the corrosion process through direct participation.

(5) Increases in CO_2 gas phase concentration above 50% accelerate corrosion in the absence of H_2S in HCO_3^- and Ca^{2+} free brine.

(6) A velocity of 7.7 mps (metres per second) may accelerate corrosion slightly at 50 mole percent H_2S and CO_2 at 150°C in the presence of HCO_3^- and Ca^{2+}.

(7) The corrosion rates of the seamless and welded grades of steel, submitted for study in this program, were similar. This implies that differences between the materials due to chemistry, heat treatment and the inclusion of welds were not significant to distinguish them by their corrosion behaviour under the current experimental conditions. General corrosion was the only type of corrosion observed.

(8) The major corrosion product, when H_2S is present, is pyrrhotite, which appeared in two stoichiometries ($Fe_{1-\chi}S$ and Fe_7S_8). Troilite (FeS) and marcasite and pyrite (FeS_2) appear to form at higher H_2S concentrations. When only carbon dioxide is present, siderite ($FeCO_3$) is formed.

(9) Corrosion rates in the vapour zone are varied. This variation is likely the result of variations in (1) the rate of condensation of water vapour and splashing of brine on the sample surface, and (2) whether the condensation or splashes form droplets or a film of liquid and (3) whether the liquid runs off or remains on the coupon surface.

7. RECOMMENDATIONS FOR FURTHER STUDY

Figure 3 graphically depicts the potential of this work to establish a family of curves relative to the behaviour of OCTG materials in brine solutions containing CO_2 to which H_2S is added. The need to

generate more data is apparent as trends predicted by this study need to be established experimentally. Therefore continuing this study, by adding points to Figure 3 which will generate family of corrosion versus H_2S (in CO_2/brine solutions) curves, is highly recommended. Such additional data will help Canada's OCTG producers to evaluate their competitive strategies for international sales.

R. W. Elliott
Project Scientist
Metals & Corrosion Technologies

R. T. Lassau
Director
Metal Technologies

REFERENCES

[1] C. De Waard and D. E. Milliams, Corrosion 31, 177 (1975).

[2] B. R. D. Gerus, SPE Preprint 5188, Symposium on Sour Gas and Cruds of the Society of Petroleum Engineers of AIME, Texas, Nov. 11-12, 1974.

TABLE I

CHEMICAL COMPOSITIONS OF TEST MATERIALS

		C	Mn	P	S	Si	Cr	Mo	Al
Algoma	K55	0.47	1.01	0.018	0.015	0.30	0.05	0.02	0.046
	L80	0.27	1.36	0.023	0.017	0.31	0.10	0.06	0.046
	S0095	0.29	1.30	0.023	0.016	0.31	0.09	0.06	0.037
IPSCO	IJW55	0.25	1.38	0.011	0.005	0.25	-	-	0.027
	IKW55	0.288	0.96	0.010	0.002	0.26	-	0.159	0.007
	ILW80	0.265	0.92	0.012	0.003	0.25	-	0.166	0.052

TABLE II

BRINE COMPOSITION

(ASTM D 1141)

The brine solution was prepared by combining 245.34 g of NaCl and 40.94 g of anhydrous Na_2SO_4 in 8 L of water. A 200 mL aliquot and a 100 mL aliquot of stock solutions No. 1 and No. 2, respectively, were added to this solution. The total solution volume was diluted to 10.0 L and the pH adjusted to 8.2 with 0.1 N NaOH. The modified brine was prepared by substituting an equimolar amount of NaCl for $CaCl_2$ and $NaHCO_3$.

Stock Solution No. 1	
$MgCl_2.6H_2O$	555.6 g/L
$CaCl_2$ (anhydrous)	57.9 g/L
$SrCl_2.6H_2O$	2.1 g/L

Stock Solution No. 2	
KC1	69.5 g/L
$NaHCO_3$	20.1 g/L
KBr	10.1 g/L
H_3BO_3	2.7 g/L
NaF	0.3 g/L

TABLE III

AUTOCLAVE EXPERIMENTS

Experiment Number	Conditions*
1	10% CO_2 60% H_2S 30% N_2 150°C
2	70% CO_2 30% H_2S 0% N_2 150°C
3	20% CO_2 20% H_2S 60% N_2 150°C
4	10% CO_2 70% H_2S 20% N_2 100°C
5	30% CO_2 60% H_2S 10% N_2 100°C
6	80% CO_2 0% H_2S 20% N_2 100°C
7	70% CO_2 30% H_2S 0% N_2 150°C ASTM D 1141 Brine
8	50% CO_2 50% H_2S 0% N_2 150°C ASTM D 1141 Brine Velocity 7.7 mps

All of these experiments, except experiments 7 and 8, were conducted using a modified ASTM D 1141 brine, in which $CaCl_2$ and $NaHCO_3$ were replaced by an equivalent number of moles of NaCl.

* Total pressure was 4000 psig; time of exposure 14 days.

TABLE IV

COUPON DEPOSIT COMPOSITION FROM X-RAY DIFFRACTION ANALYSIS

Experiment Number	Material	Coupon Deposit Composition
1	L80	Major component troilite, FeS (98%); unidentified 1 - 2%.
2	Precipitate	Major component, pyrrhotite,(a) (Fe_7S_8) (90%); Marcasite (FeS_2) (5 - 10%); Sulphur (1 - 2%); Unidentified 1 - 2%.
3	K55	Major component pyrrhotite,(a) $Fe_{1-\chi}S$, (98%); unidentified 1 - 2%.
4	K55	Major component pyrrhotite,(a) $Fe_{1-\chi}S$, (98%); unidentified 1 - 2%.
5	K55	Major component pyrrhotite,(a) Fe_7S_8 (95%); Sulphur (1 - 2%), unidentified 1 - 2%.
6	IKW55 (scrapings)	Major component siderite, $FeCO_3$ (100%).
7	K55	Major component pyrrhotite,(a) Fe_7S_8 (90%); Marcasite (FeS_2) (1 - 2%); Sulphur (S) (1 - 2%); unidentified 1 - 2%.
8	ILW80	Major component pyrrhotite,(a) $Fe_{1-x}S$ (80%), Pyrite, FeS_2 (10 - 20%); Marcasite, FeS_2 (5 - 10%); unidentified 1 - 2%.

(a) Pyrrhotite has a variable crystallographic composition.

DESCRIPTION OF TABLES V - X

Weight gain column	refers to difference in weights between "as-received" and autoclaved conditions of coupon. Gains are due to the accumulation of corrosion products on the surface.
Weight loss column	refers to difference in weights between "as-received" and descaled conditions of coupons. Losses are due to general metal corrosion and cleaning losses.

TABLE V

CORROSION RATE DATA FOR K55 SEAMLESS SPECIMENS

Coupon No.	Experiment No.	Weight Gain (mg)	Weight Loss (mg)	Corrosion Rate (mm/yr)
K-1	1	299.7	272.0	0.55
K-2	1	298.6	283.4	0.60
K-3	1	302.1	240.9	0.50
K-4	2	327.7	263.9	0.55
K-5	2	337.5	269.8	0.55
K-6	2	353.9	297.6	0.62
K-12	3	353.1	331.5	0.68
K-13	3	338.5	349.1	0.72
K-14	3	Mechanically damaged		
K-7	4	Mechanically damaged		
K-8	4	102.5	96.0	0.20
K-15	4	104.9	94.6	0.19
K-17	5	93.7	179.8	0.36
K-18	5	Mechanically damaged		
K-16	5	88.4	164.8	0.34
K-9	6	564.3	837.5	1.68
K-10	6	501.6	704.6	1.42
K-11	6	545.9	847.6	1.73
K-19	7	278.9	298.7	0.61
K-20	7	214.8	272.4	0.55
K-21	7	338.9	267.1	0.54

TABLE VI

CORROSION RATE DATA FOR L80 SEAMLESS SPECIMENS

Coupon No.	Experiment No.	Weight Gain (mg)	Weight Loss (mg)	Corrosion Rate (mm/yr)
L-1	1	310.3	273.3	0.47
L-2	1	338.7	247.2	0.48
L-3	1	347.7	257.1	0.50
L-13 (polished)	1	520.4	401.7	0.78
L-14 (polished)	1	Mechanically damaged		
L-15 (polished)	1	456.6	359.8	0.70
L-4 (vapour)	1	320.2	241.1	0.70
L-5 (vapour)	1	367.7	269.1	0.76
L-6 (vapour)	1	379.6	271.1	0.75
L-10	2	366.8	276.5	0.54
L-11	2	372.8	272.3	0.53
L-12	2	377.6	303.0	0.59
L-16 (vapour)	2	300.7	251.8	0.50
L-17 (vapour)	2	328.8	273.3	0.53
L-18 (vapour)	2	339.8	268.5	0.52
L-19	3	468.6	376.0	0.70
L-20	3	407.6	354.4	0.66
L-21	3	330.1	368.1	0.68
L-22 (vapour)	3	410.7	320.1	0.61
L-23 (vapour)	3	440.2	374.9	0.79
L-24 (vapour)	3	518.2	397.8	0.77
L-26	4	45.9	180.2	0.35
L-27	4	84.6	336.0	0.65
L-28	4	70.0	294.8	0.58
L-29 (vapour)	4	127.8	106.1	0.20
L-30 (vapour)	4	165.6	144.4	0.28
L-31 (vapour)	4	347.0	543.2	1.07

Table VI (continued)

Coupon No.	Experiment No.	Weight Gain (mg)	Weight Loss (mg)	Corrosion Rate (mm/yr)
L-32	5	100.1	195.8	0.38
L-33	5	97.1	187.6	0.36
L-34	5	Mechanically damaged		
L-35 (vapour)	5	135.1	111.5	0.21
L-36 (vapour)	5	152.5	115.9	0.22
L-37 (vapour)	5	138.7	112.7	0.22
L-7	6	766.0	1294.4	2.49
L-8	6	614.5	1060.7	2.05
L-9	6	754.0	1363.9	2.61
L-38	7	442.7	352.9	0.68
L-39	7	360.3	299.6	0.58
L-40	7	387.9	288.3	0.56
L-41 (vapour)	7	370.9	302.5	0.58
L-42 (vapour)	7	379.9	284.7	0.58
L-43 (vapour)	7	385.6	293.5	0.57

TABLE VII

CORROSION RATE DATA FOR S0095 SEAMLESS SPECIMENS

Coupon No.	Experiment No.	Weight Gain (mg)	Weight Loss (mg)	Corrosion Rate (mm/yr)
S-2	1	364.0	278.3	0.49
S-3	1	308.9	235.4	0.48
S-4	1	467.9	343.3	0.60
S-5 (vapour)	1	879.5	1107.4	2.82
S-6 (vapour)	1	472.2	344.4	0.88
S-7 (vapour)	1	536.1	358.3	0.89
S-12	2	481.0	346.0	0.61
S-13	2	425.8	303.7	0.53
S-17	2	Mechanically damaged		
S-18 (vapour)	2	370.0	287.7	0.52
S-19 (vapour)	2	368.5	300.8	0.52
S-20 (vapour)	2	359.4	291.0	0.50
S-23	3	552.1	417.4	0.73
S-24	3	534.6	427.4	0.74
S-25	3	427.8	428.4	0.74
S-15 (vapour)	3	561.4	609.7	1.27
S-21 (vapour)	3	616.1	550.8	0.96
S-22 (vapour)	3	591.4	469.8	0.82
S-26	4	67.6	252.9	0.44
S-27	4	72.8	248.6	0.43
S-28	4	81.4	280.6	0.49
S-29 (vapour)	4	262.4	206.4	0.36
S-30 (vapour)	4	325.4	229.9	0.40
S-31 (vapour)	4	203.6	174.7	0.30
S-32	5	135.3	235.8	0.41
S-33	5	115.9	218.1	0.38
S-34	5	132.1	250.0	0.43
S-35 (vapour)	5	205.7	154.8	0.27
S-36 (vapour)	5	130.0	105.2	0.18
S-37 (vapour)	5	Sample retained for analysis		

Table VII (continued)

Coupon No.	Experiment No.	Weight Gain (mg)	Weight Loss (mg)	Corrosion Rate (mm/yr)
S-8	6	723.4	1136.6	2.08
S-9	6	560.7	817.5	1.47
S-10	6	780.0	1390.2	2.41
S-38	7	456.0	354.6	0.62
S-39	7	434.3	331.8	0.58
S-40	7	469.8	352.0	0.61
S-41 (vapour)	7	412.5	325.7	0.57
S-42 (vapour)	7	451.7	353.2	0.61
S-43	7	435.0	360.7	0.63
S-46	8	334.8	299.3	0.52
S-47	8	339.0	293.8	0.51

TABLE VIII

CORROSION RATE DATA FOR IJW55 ERW SPECIMENS

Coupon No.	Experiment No.	Weight Gain (mg)	Weight Loss (mg)	Corrosion Rate (mm/yr)
IJ-1	1	344.7	247.1	0.47
IJ-2	1	322.5	256.2	0.49
IJ-3	1	345.6	283.6	0.54
IJ-4	2	307.4	243.3	0.52
IJ-5	2	362.9	286.6	0.55
IJ-6	2	375.7	316.6	0.62
IJ-10	3	239.3	308.4	0.59
IJ-11	3	364.2	303.6	0.58
IJ-12	3	369.5	276.8	0.59
IJ-13	4	146.6	116.7	0.22
IJ-14	4	152.9	144.7	0.29
IJ-15	4	159.6	160.5	0.31
IJ-16	5	97.8	153.1	0.38
IJ-18	5	96.2	168.0	0.40
IJ-19	5	85.4	168.0	0.41
IJ-7	6	606.7	873.8	1.65
IJ-8	6	543.0	741.9	1.47
IJ-9	6	558.4	715.5	1.35
IJ-20	7	366.7	294.2	0.58
IJ-21	7	425.5	334.1	0.66
IJ-22	7	314.3	289.4	0.68

TABLE IX

CORROSION RATE DATA FOR IKW55 ERW SPECIMENS

Coupon No.	Experiment No.	Weight Gain (mg)	Weight Loss (mg)	Corrosion Rate (mm/yr)
IK-1	1	655.7	815.3	1.61
IK-2	1	299.4	289.4	0.62
IK-3	1	369.1	277.9	0.60
IK-4	2	270.6	270.0	0.58
IK-5	2	466.4	358.4	0.71
IK-6	2	364.9	320.4	0.63
IK-10	3	337.8	276.8	0.59
IK-11	3	397.7	314.7	0.66
IK-12	3	428.9	333.4	0.66
IK-13	4	168.9	144.1	0.28
IK-14	4	147.0	120.0	0.23
IK-15	4	160.6	138.6	0.27
IK-17	5	135.9	186.7	0.39
IK-18	5	126.9	193.5	0.41
IK-19	5	121.7	195.3	0.41
IK-7	6	414.1	527.8	1.11
IK-8	6	434.6	549.0	1.15
IK-9	6	445.0	548.0	1.06
IK-20	7	500.8	360.2	0.76
IK-21	7	356.3	324.9	0.69
IK-22	7	298.9	330.9	0.81

TABLE X

CORROSION RATE DATA FOR ILW80 ERW SPECIMENS

Coupon No.	Experiment No.	Weight Gain (mg)	Weight Loss (mg)	Corrosion Rate (mm/yr)
IL-1	1	298.0	237.4	0.45
IL-2	1	303.2	242.1	0.46
IL-3	1	333.6	272.2	0.52
IL-13 (polished)	1	520.4	401.7	0.78
IL-14 (polished)	1	Mechanically damaged		
IL-15 (polished)	1	456.6	359.8	0.70
IL-4	2	398.5	303.4	0.67
IL-5	2	323.2	241.5	0.48
IL-6	2	334.2	254.6	0.49
IL-10	3	356.1	323.9	0.62
IL-11	3	356.3	299.7	0.57
IL-12	3	429.1	325.4	0.70
IL-16	4	92.2	103.2	0.22
IL-17	4	143.7	150.5	0.26
IL-18	4	191.4	197.9	0.37
IL-19	5	95.2	194.6	0.37
IL-20	5	98.4	199.6	0.38
IL-21	5	94.7	191.3	0.37
IL-7	6	476.7	562.3	1.19
IL-8	6	438.6	536.0	1.00
IL-9	6	467.7	634.6	1.19
IL-22	7	361.0	284.1	0.54
IL-23	7	448.3	355.3	0.67
IL-24	7	373.0	350.0	0.66
IL-27	8	240.2	212.1	0.37
IL-28	8	257.9	238.7	0.41

TABLE XI

AVERAGE CORROSION RATES (mm/yr) AND 90% CONFIDENCE LIMIT FROM t-DISTRIBUTION

Carbon Steel	Experiment 1	2	3	4	5	6	7	8[d]
K55	0.55±0.06	0.57±0.04	0.70[a]	0.13[a]	0.35[a]	1.61±0.18	0.56±0.04	-
L80	0.48±0.02	0.55±0.04	0.68±0.02	0.52±0.17	0.37[a]	2.38±0.32	0.60±0.07	-
L80 (vapour)	0.74±0.04	0.51±0.02	0.69±0.10	0.24[b]	0.22±0.01	-	0.57±0.01	-
L80 (polished)	0.74[a]	-	-	-	-	-	-	-
S0095	0.52±0.08	0.57[a]	0.74±0.01	0.45±0.03	0.41±0.03	1.98±0.52	0.60±0.02	0.51
S0095 (vapour)	0.88[b]	0.51±0.01	1.05±0.25	0.33±0.05	0.23[c]	-	0.60±0.04	-
IJW55	0.50±0.04	0.56±0.05	0.59±0.01	0.27±0.05	0.40±0.01	1.49±0.16	0.64±0.06	-
IKW55	0.61[b]	0.64±0.07	0.64±0.04	0.26±0.03	0.40±0.01	1.10±0.05	0.75±0.07	-
ILW80	0.48±0.04	0.55±0.12	0.63±0.07	0.28±0.09	0.37±0.01	1.13±0.11	0.62±0.08	0.39
ILW80 (polished)	0.75±0.17	-	-	-	-	-		

a Average of two coupons, third mechanically damaged.
b Average of two coupons, third suffered accelerated attack.
c Average of two coupons, third retained for deposit analysis.
d Average of two coupons, velocity experiment.

TABLE XII

SUMMARY[a] OF THE RESULTS FROM ALL THREE PROGRAMS

Program[b] & Exp't No.	Temp. (°C)	Duration (days)	Brine	H_2S (%)	CO_2 (%)	Corrosion Rates: Avg. S'less (mm/yr)	Corrosion Rates: Avg. ERW (mm/yr)	Corrosion Rates: Avg. (mm/yr)
I-2	150	28	D 1141	0	0	0.26	0.15	0.21
I-5	150	28	Modified	0	50	0.17	0.15	0.16
I-4	100	28	D 1141	0	50	0.12	0.05	0.08
I-3	150	28	D 1141	0	50	0.06	0.10	0.08
III-6	100	14	Modified	0	80	1.99	1.24	1.62
II-1	150	21	Modified	10	50	0.39	0.31	0.35
III-3	150	14	Modified	20	20	0.71	0.62	0.66
III-2	150	14	Modified	30	70	0.56	0.58	0.57
III-7	150	14	D 1141	30	70	0.59	0.67	0.63
II-4	100	13	D 1141	50	50	0.33	0.30	0.31
II-3	150	13	D 1141	50	50	0.38	0.44	0.41
III-8[c]	150	14	D 1141	50	50	0.51	0.39	0.45
II-2	150	13	Modified	50	50	1.02	1.04	1.03
III-1	150	14	Modified	60	10	0.52	0.53	0.52
III-5	100	14	Modified	60	30	0.38	0.39	0.38
III-4	100	14	Modified	70	10	0.37	0.27	0.32

Note: (a) These data are presented graphically in Figures 2 and 3.

(b) I - Program I - Report No. 57-10486, January 27, 1987
II - Program II - Report No. 57-10731, April 30, 1988
III - Program III - This work

(c) Velocity Experiment

TABLE XIII

CORRELATION OF CORROSION RESISTANCE AND CORROSION RATE

Relative Corrosion Resistance	Corrosion Rate (mm/yr)
Outstanding	<0.02
Excellent	0.02 - 0.1
Good	0.1 - 0.5
Fair	0.5 - 1.0
Poor	1.0 - 5.0
Unacceptable	5+

Note: Data from this table were produced from Fontana, M. G. and Greene, N. D., "Corrosion Engineering", McGraw Hill Book Company, New York, 1978.

Figure 1

Schematic Drawing of Hastelloy-C Autoclave

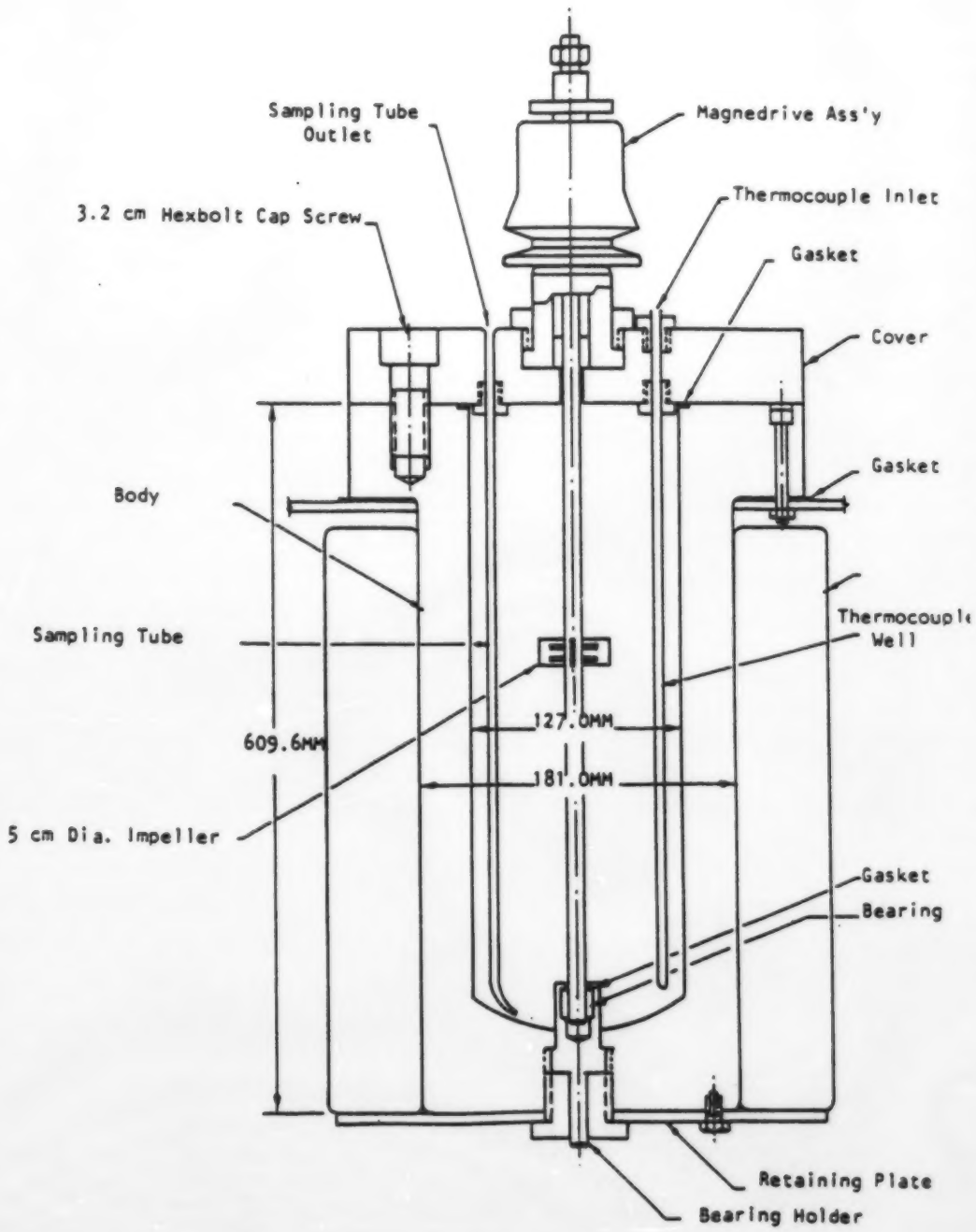

Effect of CO_2/H_2S on Seamless and ERW Tubular Goods
For C & M Engineering Ltd.

Figure 2

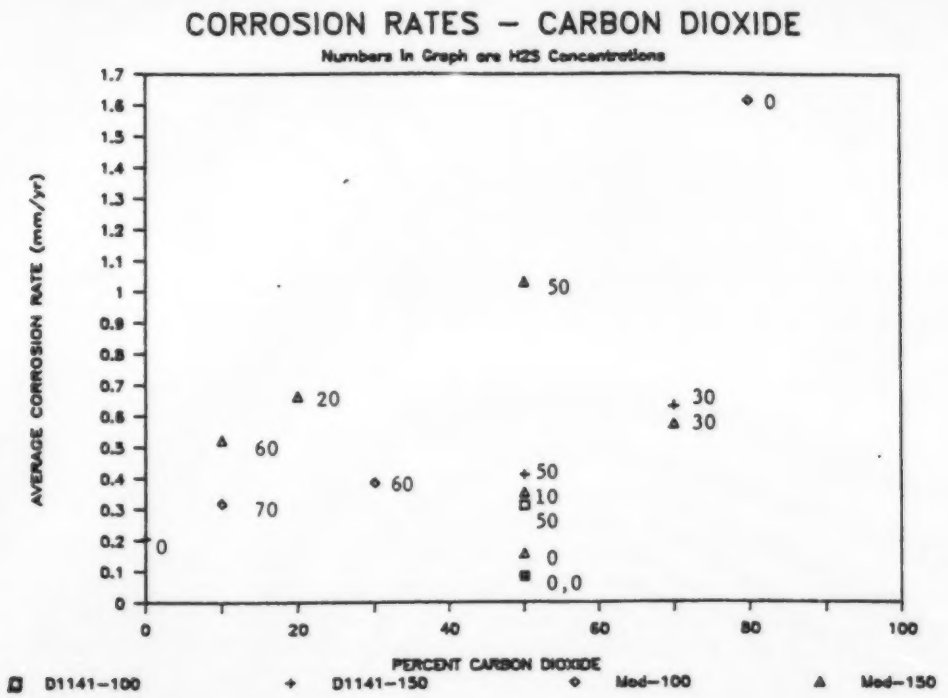

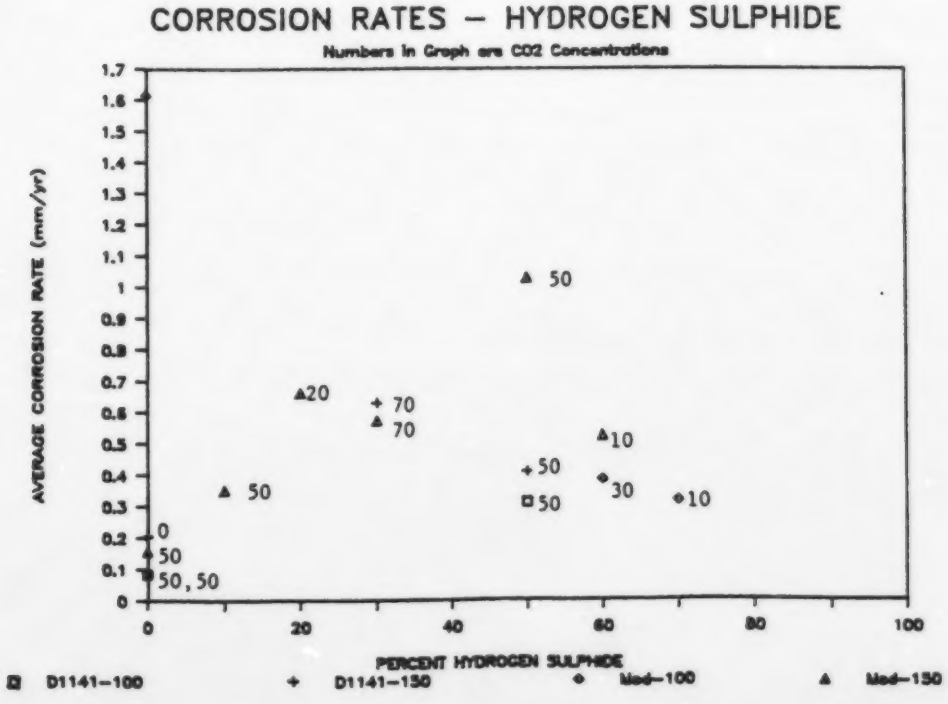

Effect of CO_2/H_2S on Seamless and ERW Tubular Goods
For C & M Engineering Ltd.

Figure 3

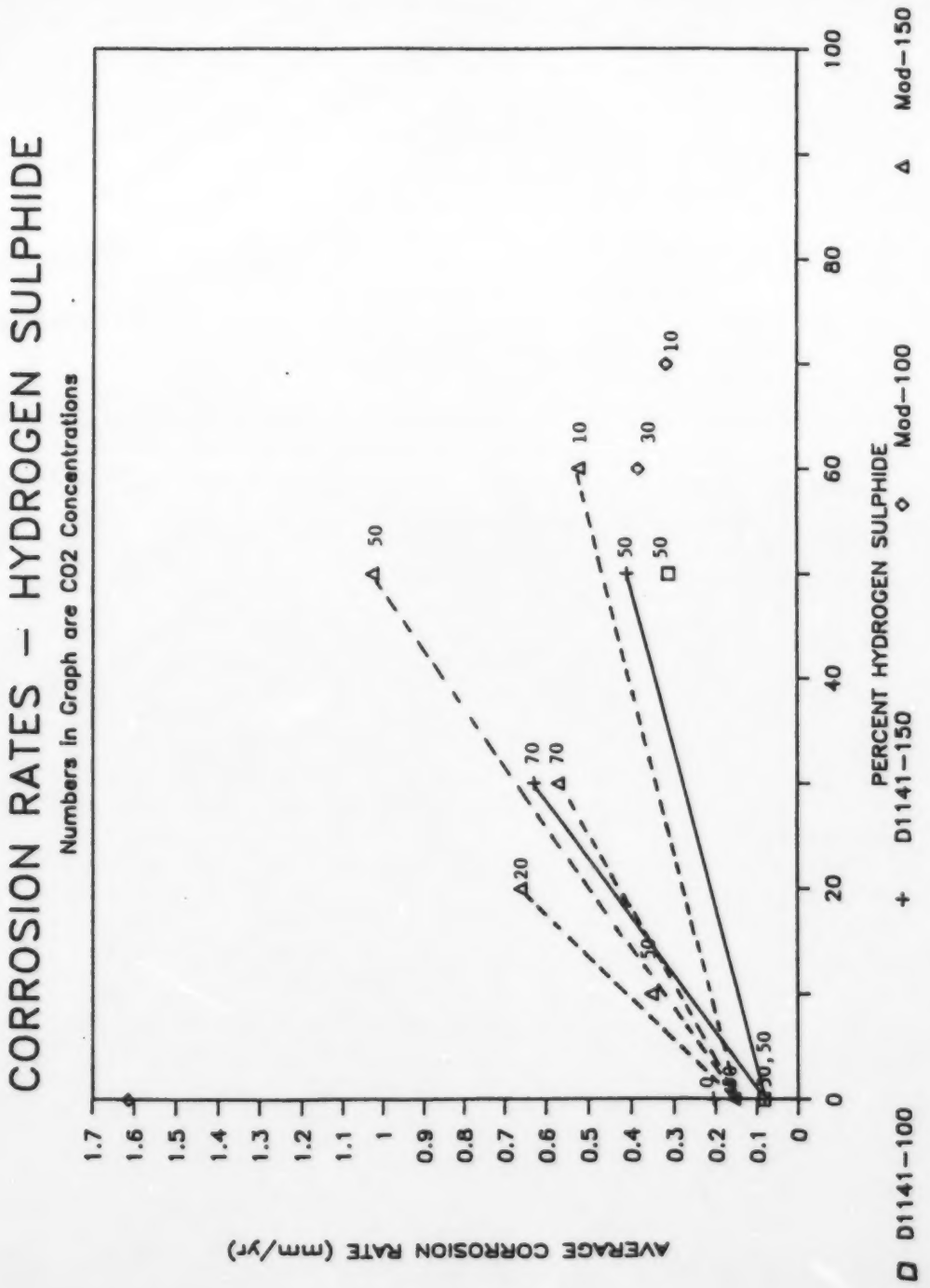

APPENDIX I: Results of Metallographic Examination

There was essentially no difference in the form of surface attack observed in the eight experiments. Representative coupons from Experiments 1 and 2, showing various forms of surface attack, were photographed. These, and other coupons from each of Experiments 1 and 2, were cross-sectioned longitudinally with some also being sectioned transversely. The corrosion observed and the photographs and photomicrographs are discussed by alloy type. The experimental conditions for each experiment are listed in Table III in the body of this report.

K55

The K55 material experienced corrosion rates of about 0.2 - 0.4 mm/year in Experiments 4 and 5; 0.6 mm/year in Experiments 1, 2 and 7; 0.7 mm/year in Experiment 3 and 1.6 mm/year in Experiment 6. The metal loss was uniform. No pitting or concentrated forms of metal loss were observed. Figure 4 is a photomicrograph of a cross-section of coupon K5 exposed in Experiment 2. There was no selective attack of the ferrite-rich zones.

L80

The L80 material had corrosion rates in the range 0.4 - 0.7 mm/year in all but Experiment 6 which gave a corrosion rate of 2.4 mm/year. The coupons experienced uniform metal loss. Photomicrographs of coupons L2 (Experiment 1) and L11 (Experiment 2) appear as Figures 5 and 6, respectively.

The L80 material, with a 320 grit polished surface rather than a glass beaded surface, experienced a corrosion rate of about 0.7 mm/yr in Experiment 1. The surface of the coupons was mottled following cleaning. This may be an effect of the high H_2S concentration. Figure 7 is a photograph of coupon L15. Figures 8 and 9 are longitudinal and transverse cross-sections, respectively, of coupon L15.

The L80 material experienced corrosion rates of 0.2 - 0.7 mm/yr in the vapour phase. Coupon L31 had a corrosion rate of 1.1 mm/year in the vapour phase, while the other two coupons had corrosion rates in the range 0.2 - 0.3 mm/year. The form of attack was general corrosion with some slight pitting. Figures 10 and 11 are photomicrographs of longitudinal cross-sections of coupons L5 (Experiment 1) and L17 (Experiment 2), respectively.

S0095

The S0095 material experienced corrosion rates in the range of 0.4 - 0.7 mm/yr in all experiments but number 6, which gave a corrosion rate of 2.0 mm/yr. The form of attack was mainly general corrosion with the formation of some very minor pits. Some of the coupons also had depressions in them following cleaning. Figures 12 and 13 are a photograph and a photomicrograph, respectively, of a longitudinal cross-section of coupon S2 which experienced uniform corrosion, respectively exposed in Experiment 1. Figures 14 and 15 are a photograph and a photomicrograph respectively of a longitudinal cross-section of coupon S13 which experienced formation of depressions in its surface, exposed in Experiment 2.

The S0095 material experienced corrosion rates of 0.2 - 0.9 mm/yr in the vapour phases. One coupon, S5, experienced a much higher corrosion rate of 2.8 mm/yr in the vapour phase of Experiment 1. The form of attack was general corrosion with some pitting in the 150°C experiments. Figures 16 and 17 are a photograph and a photomicrograph, respectively of a longitudinal cross-section of coupon S5. This mottled attack appears to be the result of condensation on the coupon surface. Figure 18 is a photomicrograph of a longitudinal cross-section of coupon S19 exposed in the vapour phase of Experiment 2.

IJW55

The IJW55 material experienced corrosion rates of 0.3 - 0.6 mm/yr in all but Experiment 6, which had a corrosion rate of 1.5 mm/year.. The form of

corrosion was general with some broad pits occurring in Experiment 7. Minor attack in the banded structure is apparent in Experiment 2 where the bands rise to the surface near the weld. Figures 19 and 20 are photomicrographs of a longitudinal cross-section of coupon IJ2 (exposed in Experiment 1) remote from and at the weld, respectively.

There was slight etching of the welds in Experiments 2, 5, 6 and 7. Figures 21 and 22 are photomicrographs of a longitudinal cross-section of coupon IJ5 (exposed in Experiment 2) remote from and at the weld, respectively. The welds were not etched in the coupons exposed in Experiment 3.

IKW55

The IKW55 material experienced corrosion rates in the range 0.3 - 0.7 mm/yr, except in Experiment 6 in which the corrosion rate was 1.1 mm/year. IK1 experienced a much higher corrosion rate of 1.6 mm/yr in Experiment 1 and was excluded from the average. The form of attack was general corrosion with transverse striations, indicating remnant rolling effects, in Experiments 2, 3 and 6, and some pitting. There was some preferential attack of the dark phase in the banded structure where the bands rise to the surface near the welds. Figure 23 is a photograph of coupon IK1 which experienced a higher corrosion rate than the other two coupons in Experiment 1. Figures 24 and 25 are photomicrographs of a longitudinal cross-section of coupon IK1 remote from and at the weld, respectively. Figures 26 and 27 and Figures 28 and 29 are the corresponding photomicrographs for coupons IK6 and IK5 (showing a depression) exposed in Experiment 2.

ILW80

The ILW80 material experienced corrosion rates in the range 0.3 - 0.6 mm/yr except in Experiment 6 in which the corrosion rate was 1.1 mm/year. The form of corrosion attack was general corrosion with the formation of depressions and some slight pitting. The welds were unetched except in the coupons exposed

in Experiment 6. Figures 30 and 31 are photomicrographs of a longitudinal cross-section of coupon IL2 remote from and at the weld, respectively, exposed in Experiment 1. Figure 32 is a photograph of coupon IL4 exposed in Experiment 2 showing the depression formed. Figures 33 and 34 are photomicrographs of a longitudinal cross-section of coupon IL4 remote from and at the weld which experienced more pitting in Experiment 2 than coupon IL6 whose corresponding photomicrographs appear as Figures 35 and 36.

The ILW80 material having a 320 grit polished surface rather than a glass beaded surface finish experienced a corrosion rate of 0.8 mm/yr in Experiment 1. The attack was general corrosion with the formation of fissures Figure 37 is a photograph of coupon IL15, and Figure 38 is a photomicrograph of a transverse cross-section of coupon IL15. Figures 39 and 40 are photomicrographs of a longitudinal cross-section of coupon IL15 remote from and at the weld, respectively. The reason for the formation of these fissures which only occurred with these coupons is not apparent. It is possible that they are hot tears originating in the heat treatment process and existed in the coupons prior to exposure but were not detected.

Figure 4

Photomicrograph of Coupon K5 (Experiment 2)

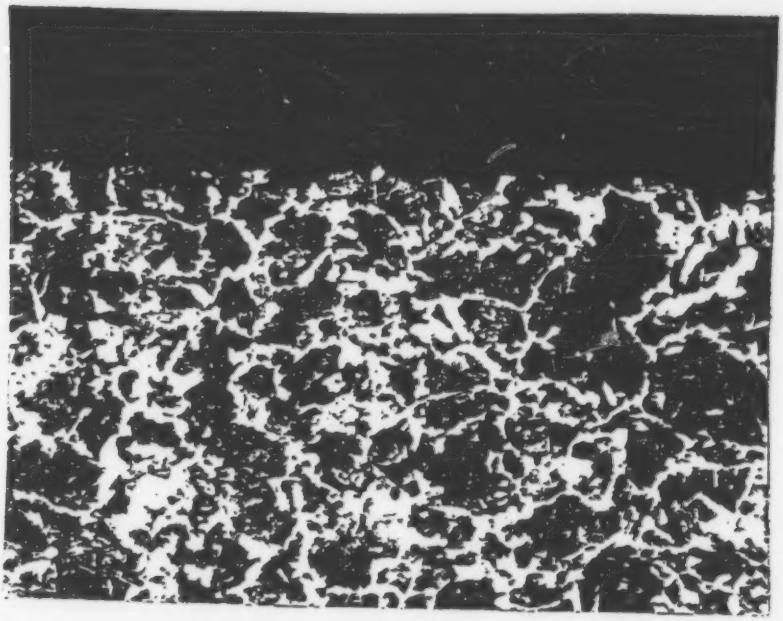

200X Magnification
Etched in 2% Nital

70% CO_2, 30% H_2S,
150°C, Modified Brine

Figure 5

Photomicrograph of Coupon L2 (Experiment 1)

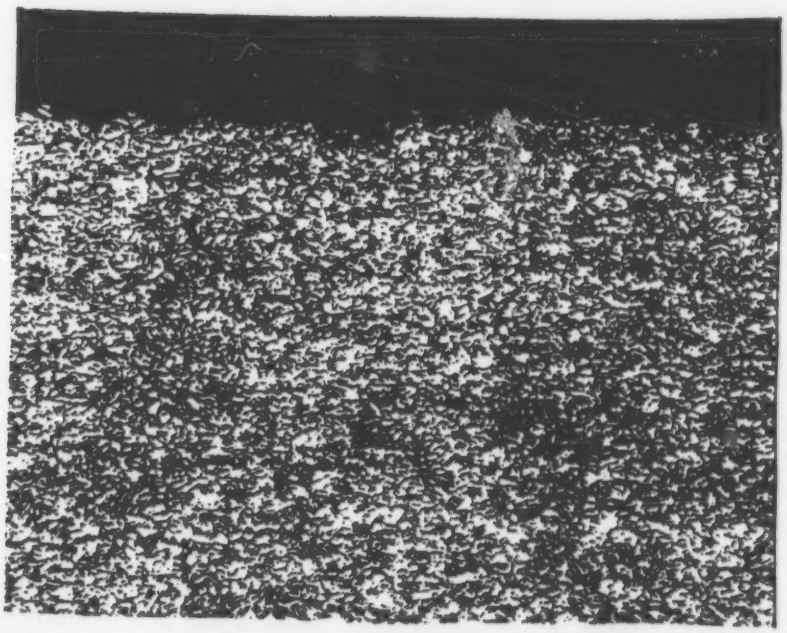

200X Magnification
Etched in 2% Nital

10% CO_2, 60% H_2S,
30% N_2, 150°C
Modified Brine

Figure 6

Photomicrograph of Coupon L11 (Experiment 2)

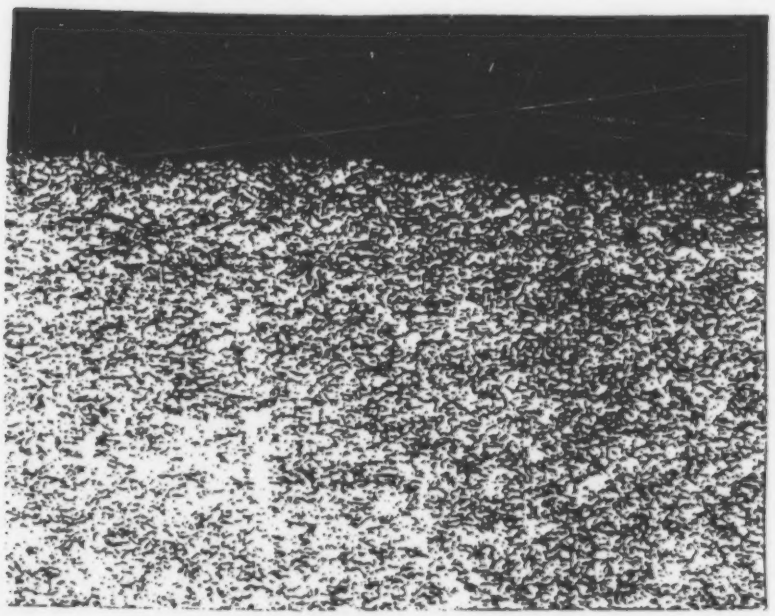

200X Magnification
Etched in 2% Nital

70% CO_2, 30% H_2S,
150°C, Modified Brine

Figure 7

Photograph of Polished Coupon L15 (Experiment 1)

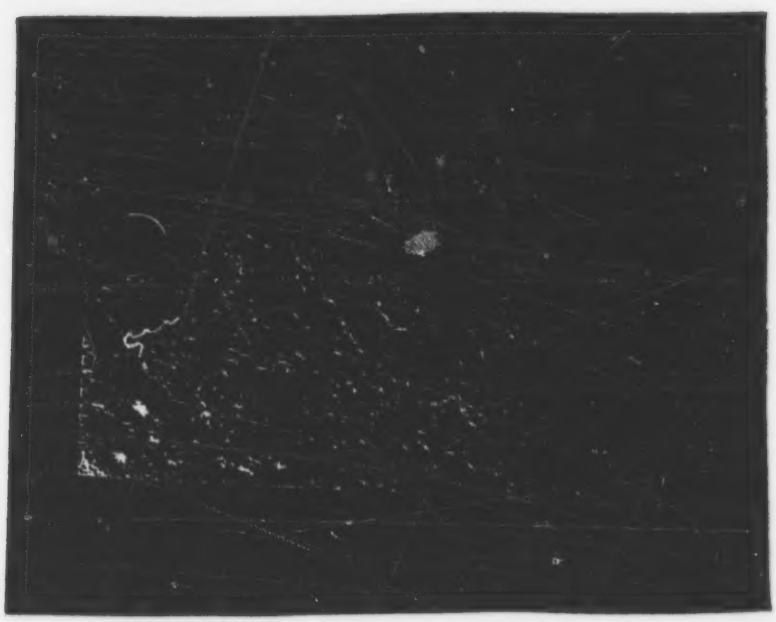

2.7X Magnification
Etched in 2% Nital

10% CO_2, 60% H_2S,
30% N_2, 150°C
Modified Brine

Figure 8

Photomicrograph of Polished Coupon L15 (Experiment 1)

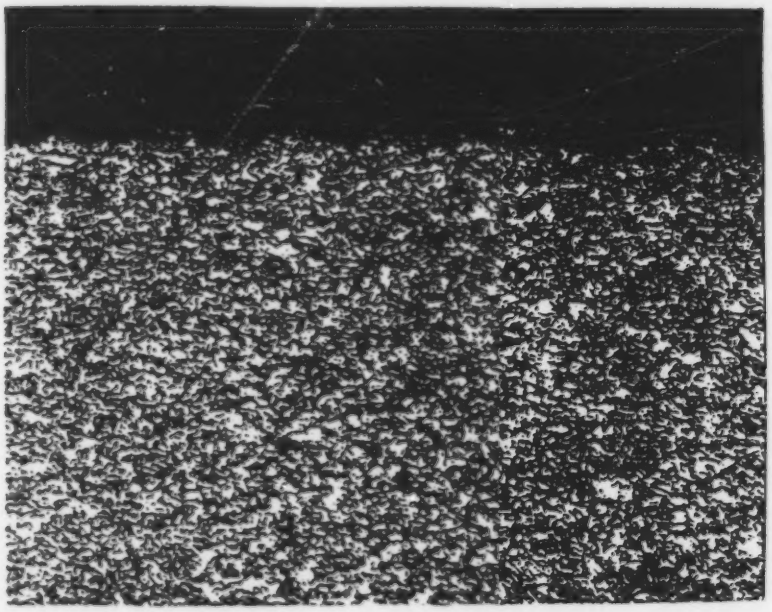

200X Magnification
Etched in 2% Nital

Longitudinal
Cross-section

Figure 9

Photomicrograph of Polished Coupon L15 (Experiment 1)

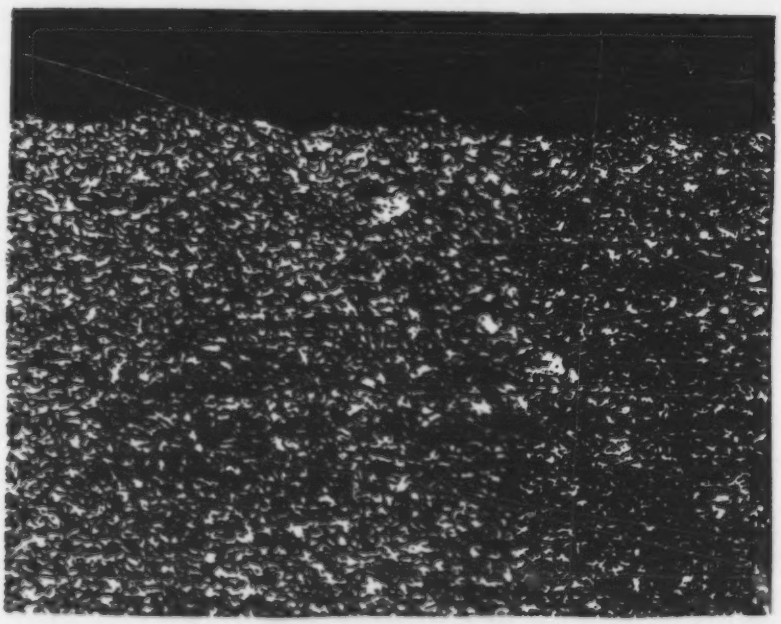

200X Magnification
Etched in 2% Nital

Transverse
Cross-section

Figure 10

Photomicrograph of Coupon L5 (Experiment 1, Vapour)

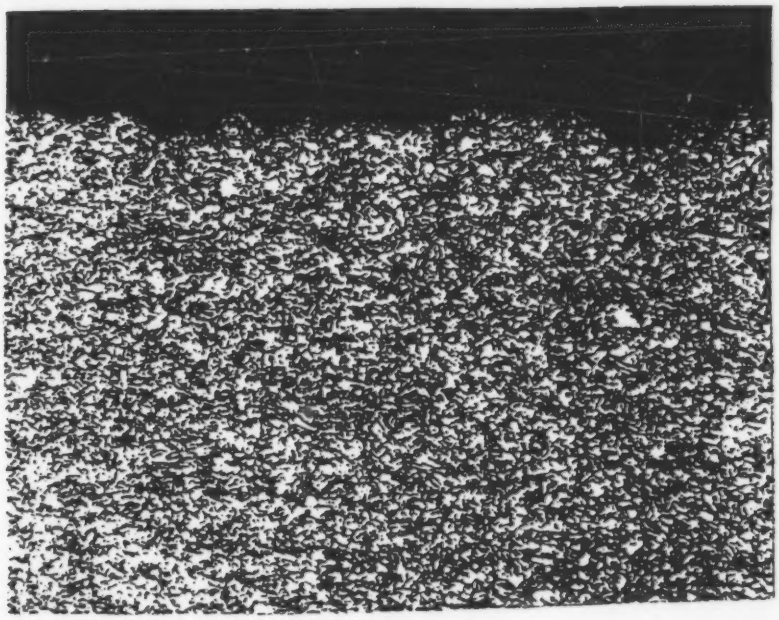

200X Magnification
Etched in 2% Nital

10% CO_2, 60% H_2S,
30% N_2, 150°C
Modified Brine

Figure 11

Photomicrograph of Coupon L17 (Experiment 2, Vapour)

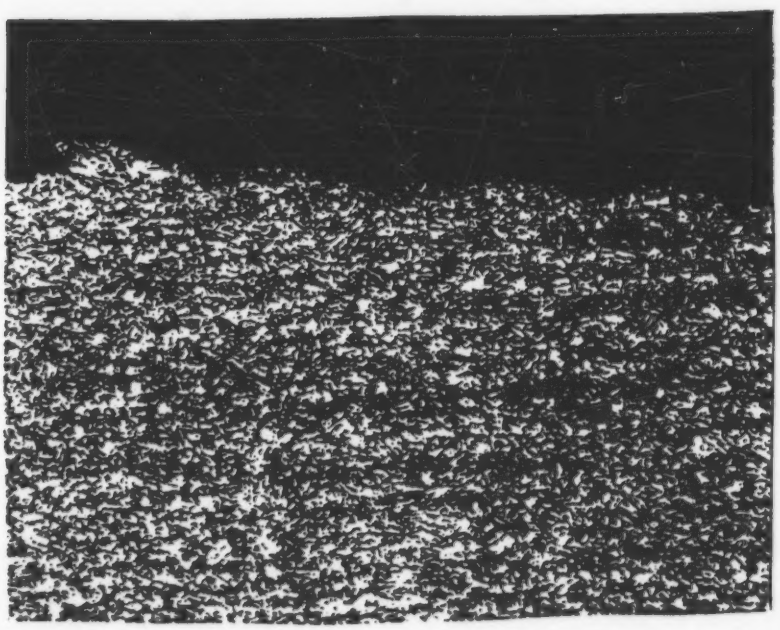

200X Magnification
Etched in 2% Nital

70% CO_2, 30% H_2S,
150°C
Modified Brine

Figure 12

Photograph of Coupon S2 (Experiment 1)

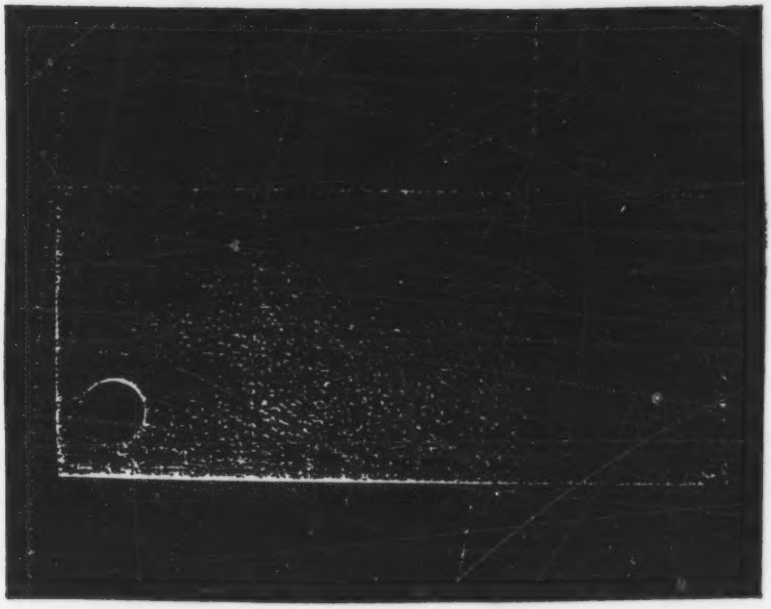

2.7X Magnification
Etched in 2% Nital

10% CO_2, 60% H_2S,
30% N_2, 150°C
Modified Brine

Figure 13

Photomicrograph of Coupon S2 (Experiment 1)

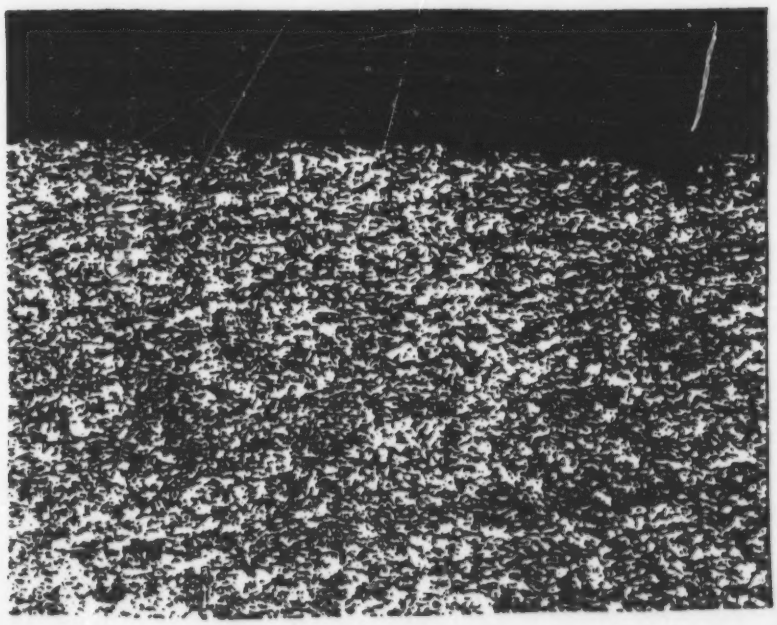

200X Magnification
Etched in 2% Nital

Figure 14

Photograph of Coupon S13 (Experiment 2)

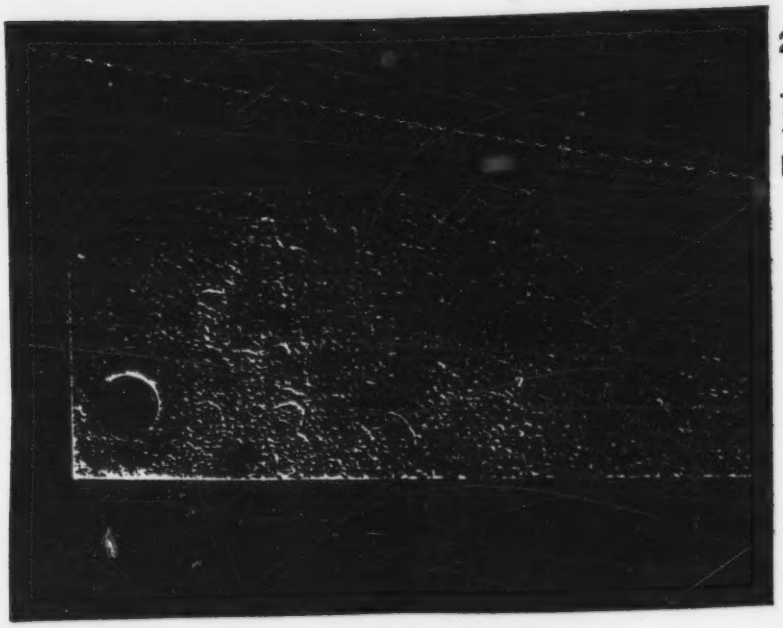

2.7X Magnification

70% CO_2, 30% H_2S,
150°C
Modified Brine

Figure 15

Photomicrograph of Coupon S13 (Experiment 2)

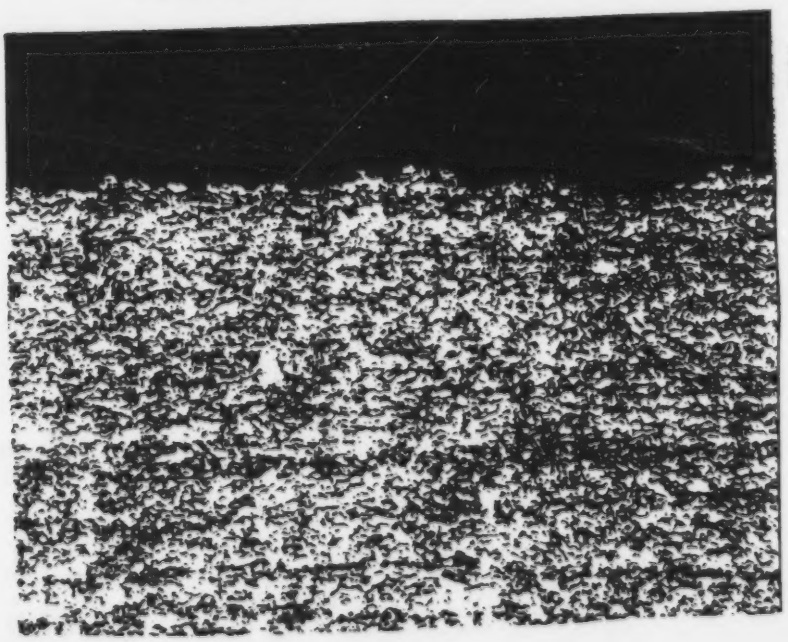

200X Magnification
Etched in 2% Nital

Figure 16

Photograph of Coupon S5 (Experiment 1, Vapour)

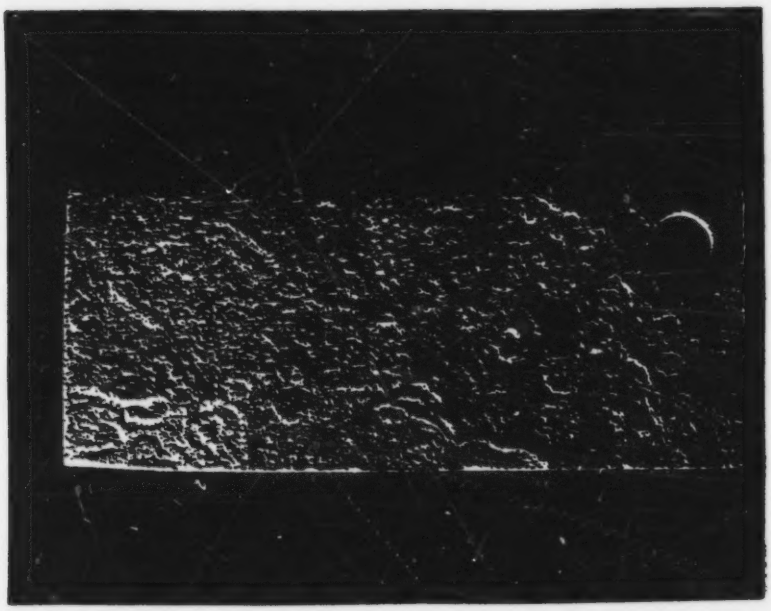

2.7X Magnification

10% CO_2, 60% H_2S, 30% N_2, 150°C Modified Brine

Figure 17

Photomicrograph of Coupon S5

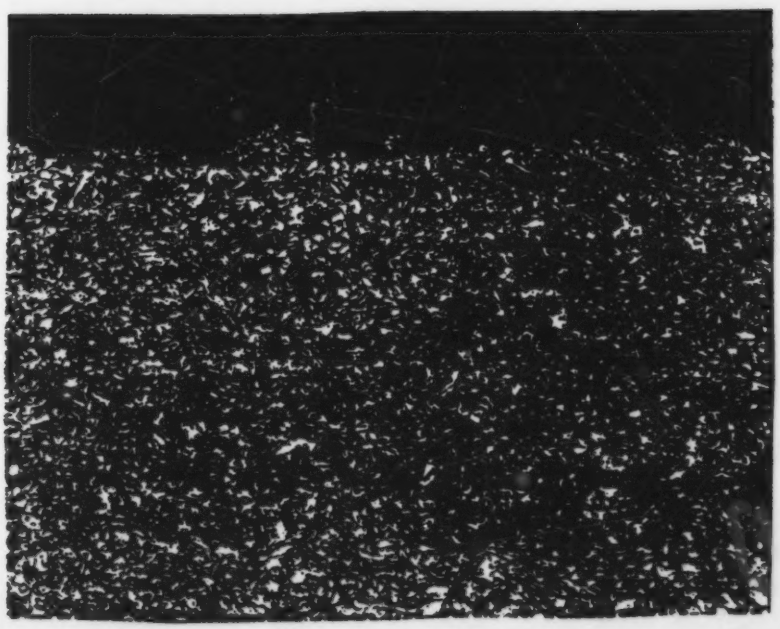

200X Magnification
Etched in 2% Nital

Figure 18

Photomicrograph of Coupon S19 (Experiment 2, Vapour)

200X Magnification

70% CO_2, 30% H_2S,
150°C
Modified Brine

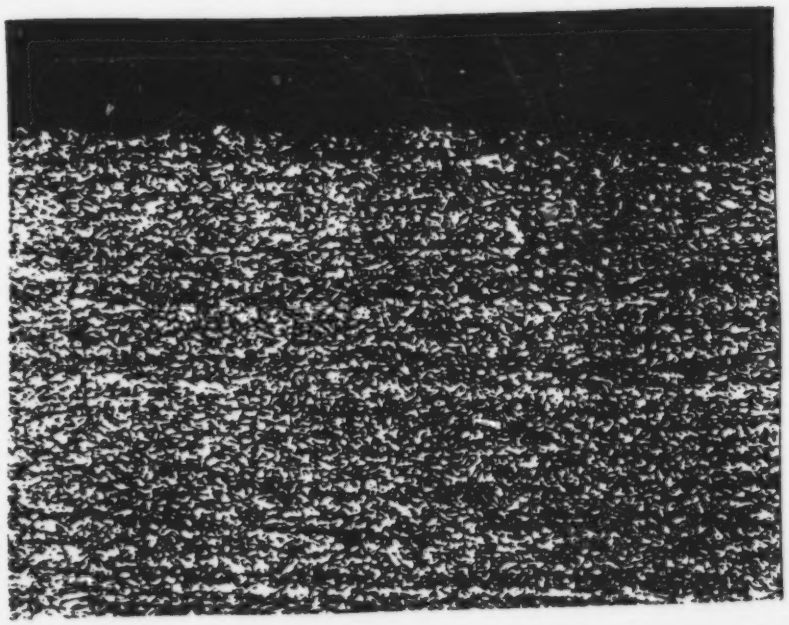

Figure 19

Photomicrograph of Coupon IJ2 Remote from Weld (Experiment 1)

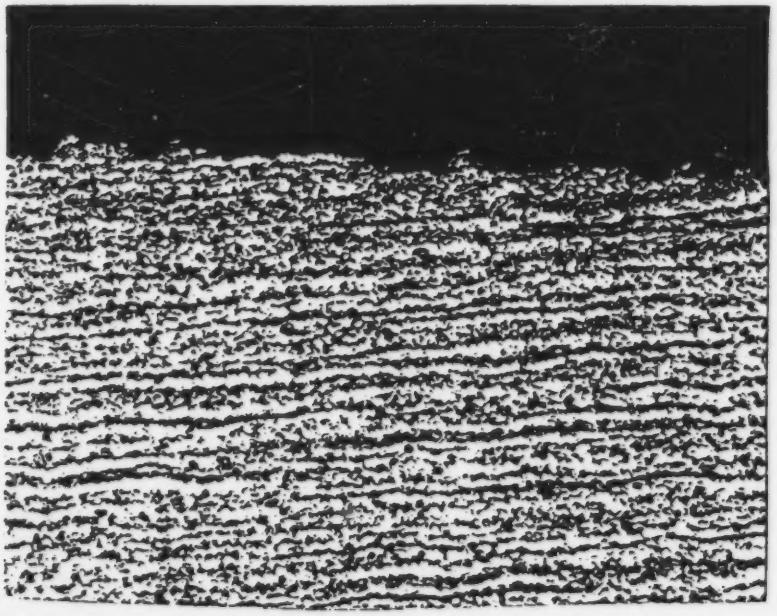

200X Magnification
Etched in 2% Nital

10% CO_2, 60% H_2S,
30% N_2, 150°C
Modified Brine

Figure 20

Photomicrograph of Coupon IJ2 at the Weld

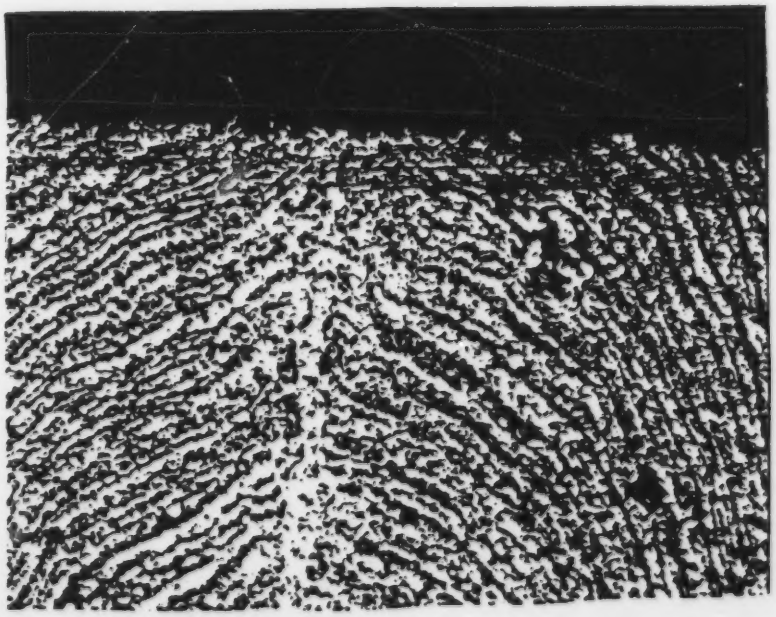

200X Magnification
Etched in 2% Nital

Figure 21

Photomicrograph of Coupon IJ5 Remote from Weld (Experiment 2)

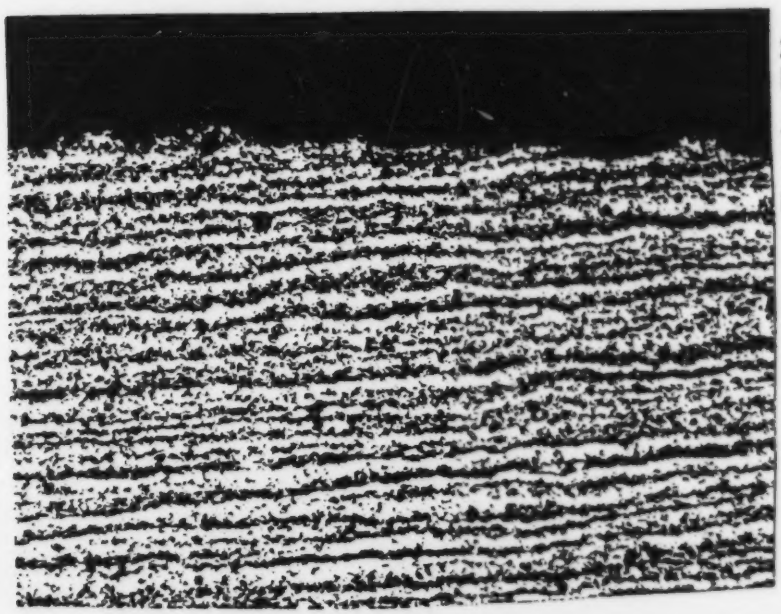

200X Magnification
Etched in 2% Nital

70% CO_2, 30% H_2S,
150°C
Modified Brine

Figure 22

Photomicrograph of Coupon IJ5 at the Weld

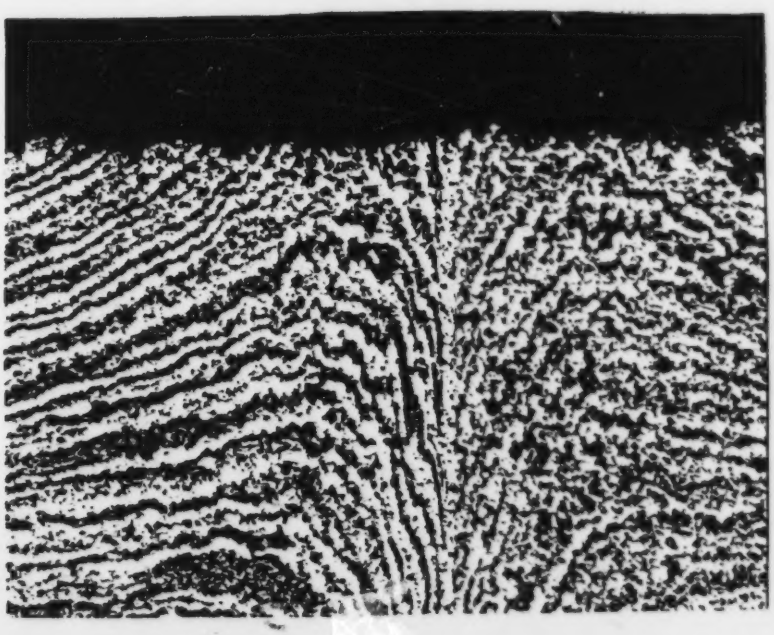

200X Magnification
Etched in 2% Nital

Figure 23

Photograph of Coupon IK1 (Experiment 1)

2.7X Magnification

10% CO_2, 60% H_2S,
30% N_2, 150°C
Modified Brine

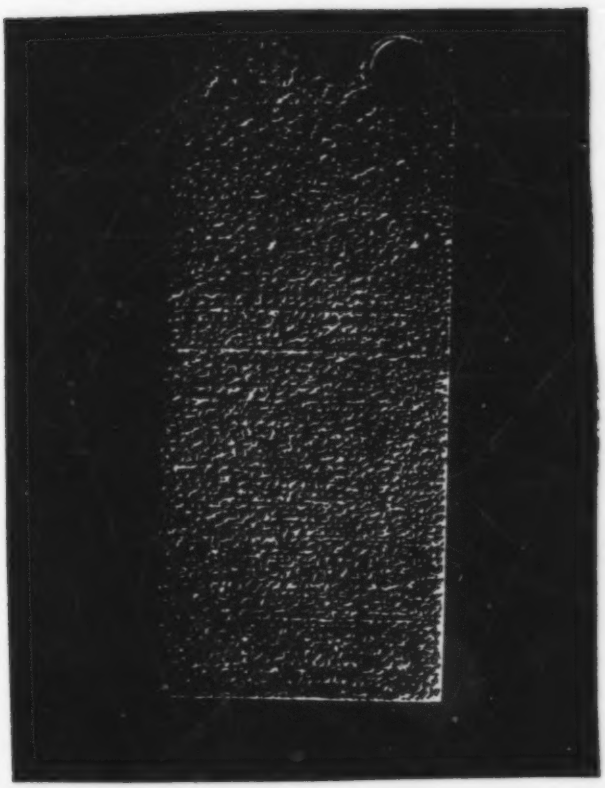

Figure 24

Photomicrograph of Coupon IK1 Remote from Weld (Experiment 1)

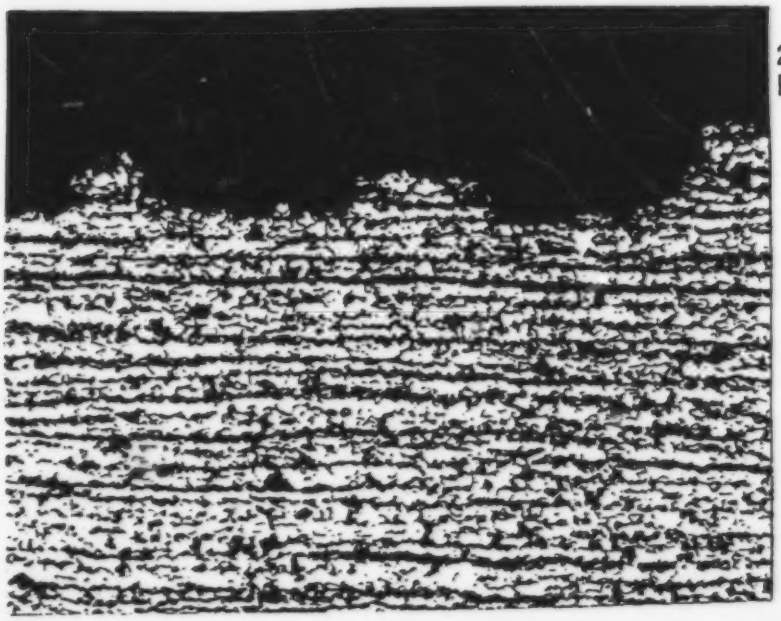

200X Magnification
Etched in 2% Nital

Figure 25

Photomicrograph of Coupon IK1 at the Weld

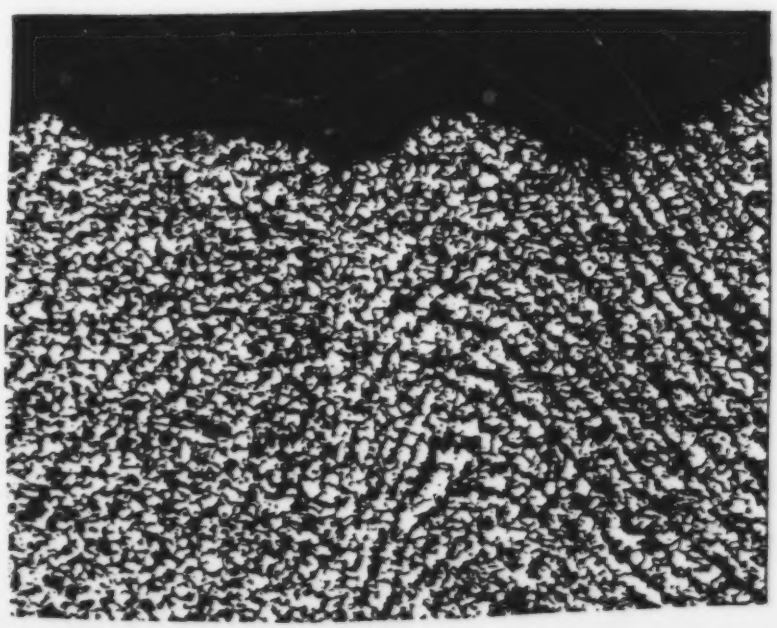

200X Magnification
Etched in 2% Nital

Figure 26

Photomicrograph of Coupon IK6 Remote from Weld (Experiment 2)

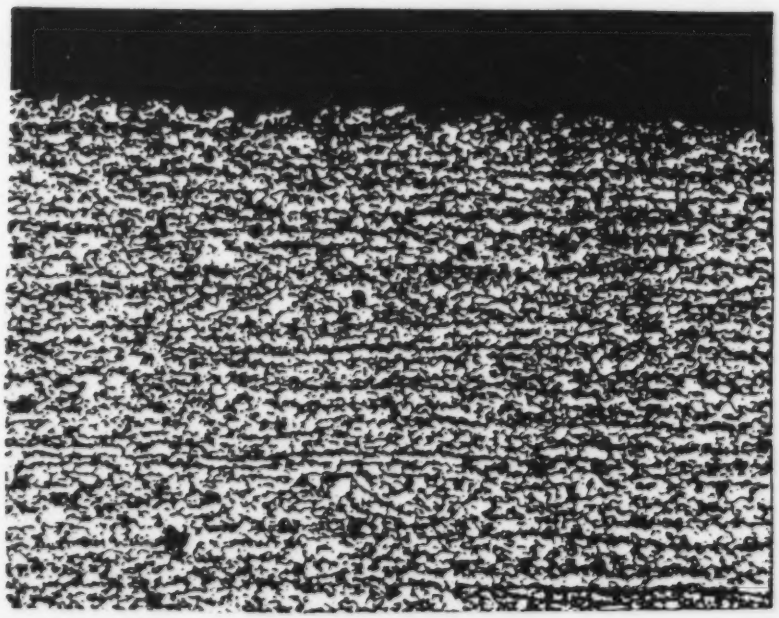

200X Magnification
Etched in 2% Nital

70% CO_2, 30% H_2S,
150°C
Modified Brine

Figure 27

Photomicrograph of Coupon IK6 at the Weld

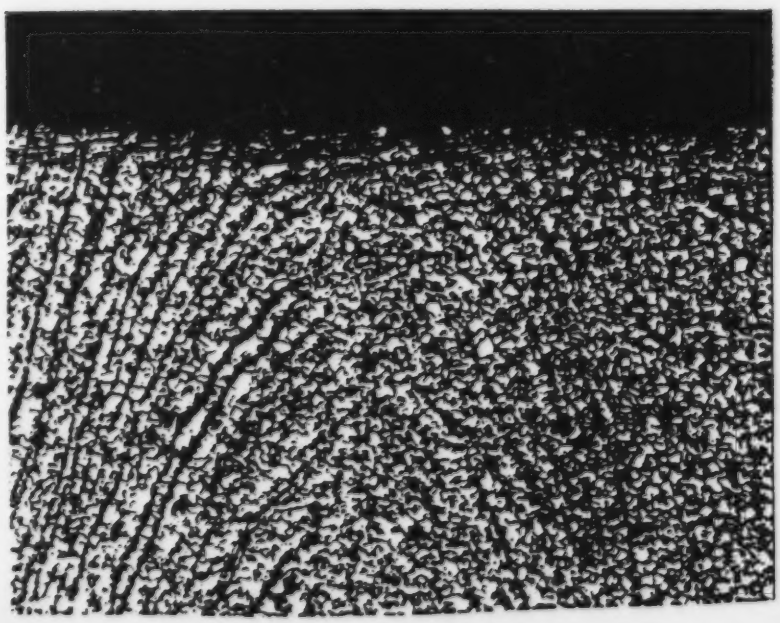

200X Magnification
Etched in 2% Nital

Figure 28

Photomicrograph of Coupon IK5 Remote from Weld (Experiment 2)

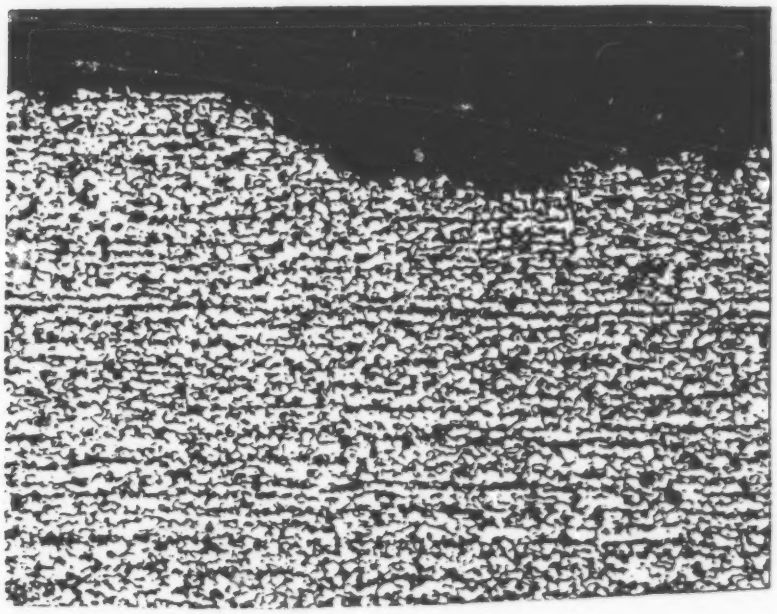

200X Magnification
Etched in 2% Nital

Figure 29

Photomicrograph of Coupon IK5 at the Weld

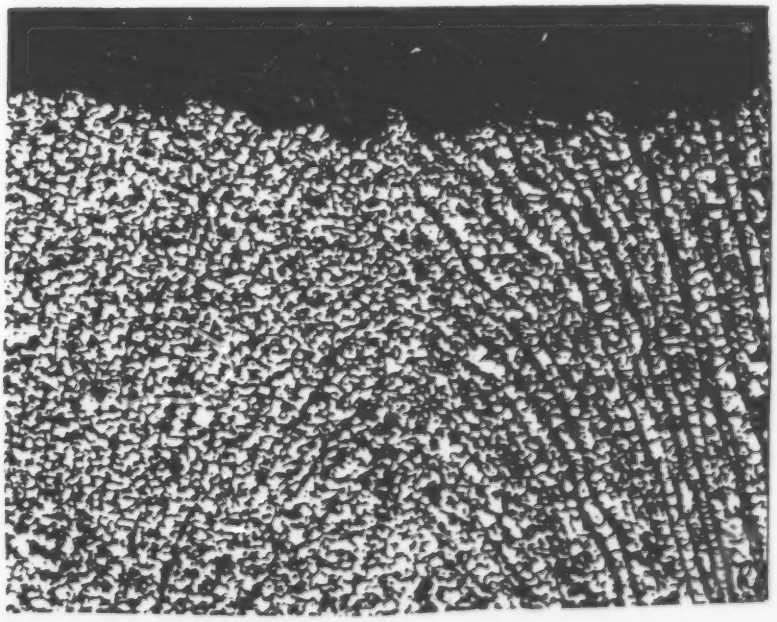

200X Magnification
Etched in 2% Nital

Figure 30

Photomicrograph of Coupon IL2 Remote from Weld (Experiment 1)

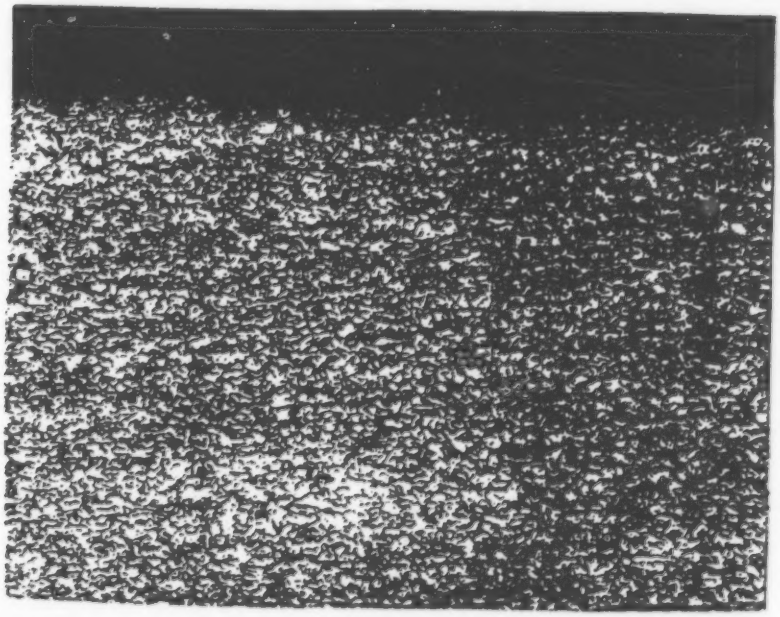

200X Magnification
Etched in 2% Nital

10% CO_2, 60% H_2S,
30% N_2, 150°C
Modified Brine

Figure 31

Photomicrograph of Coupon IL2 at the Weld

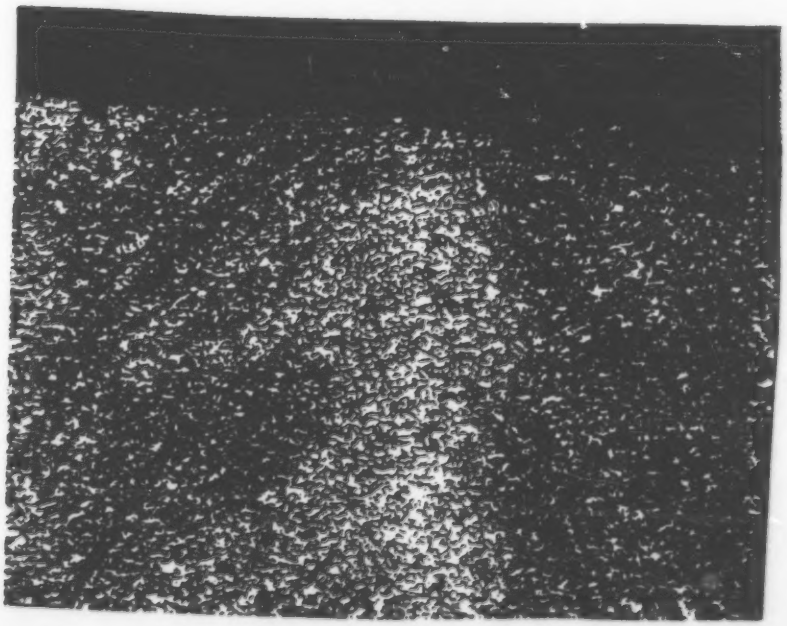

200X Magnification
Etched in 2% Nital

Figure 32

Photograph of Coupon IL4 (Experiment 2)

2.7X Magnification

70% CO_2, 30% H_2S,
150°C
Modified Brine

Figure 33

Photomicrograph of Coupon IL4 Remote from Weld (Experiment 2)

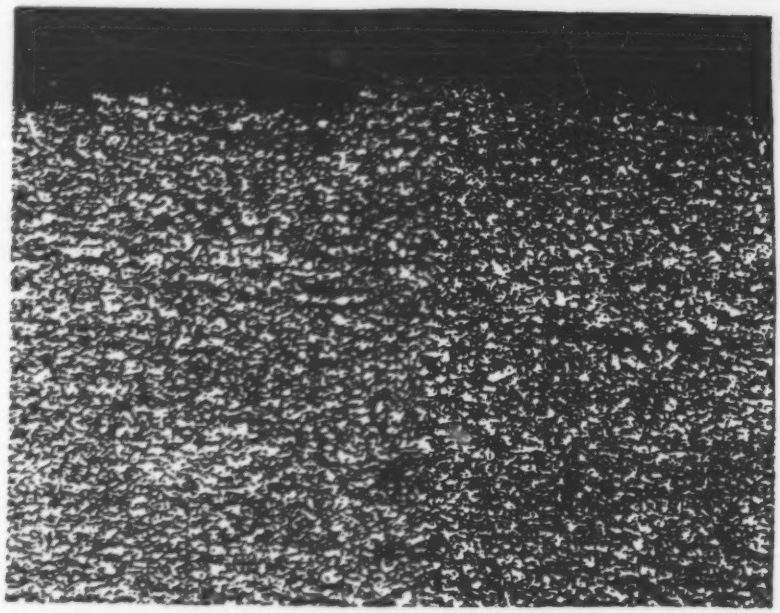

200X Magnification
Etched in 2% Nital

Figure 34

Photomicrograph of Coupon IL4 at the Weld

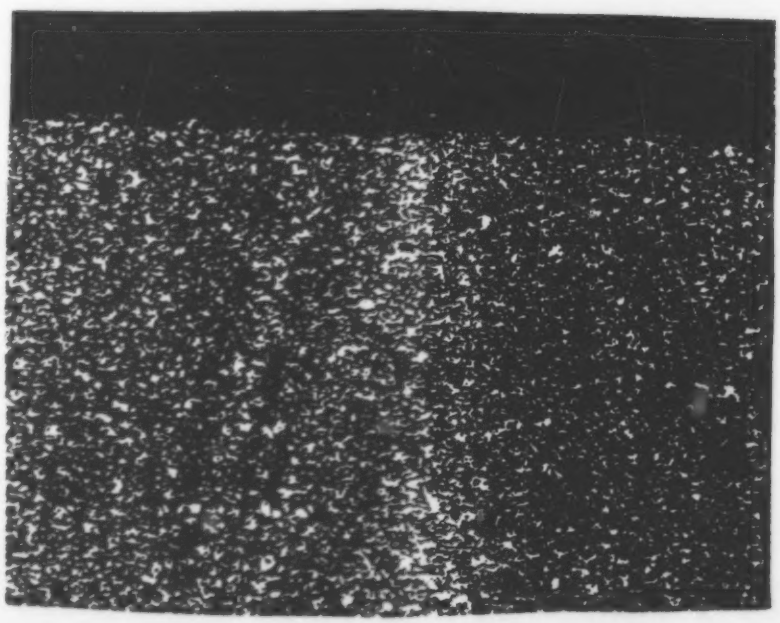

200X Magnification
Etched in 2% Nital

Figure 35

Photomicrograph of Coupon IL6 Remote from Weld (Experiment 2)

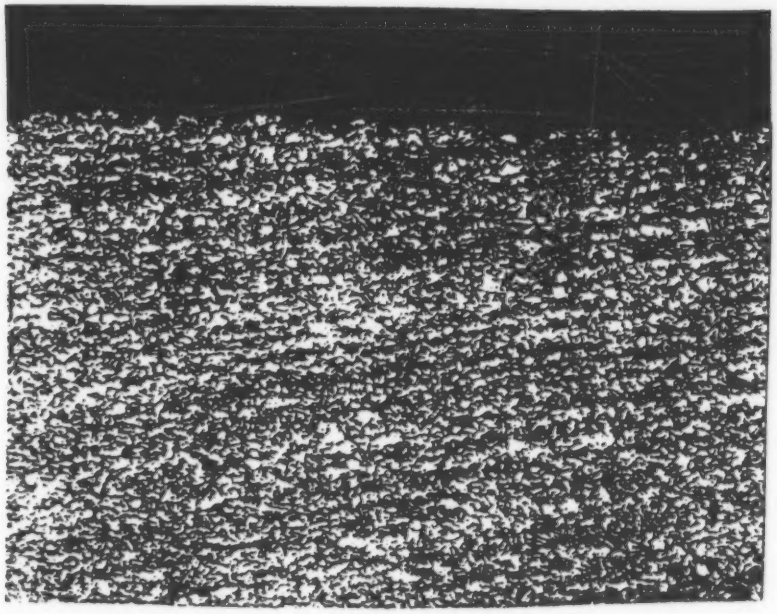

200X Magnification
Etched in 2% Nital

Figure 36

Photomicrograph of Coupon IL6 at the Weld (Experiment 2)

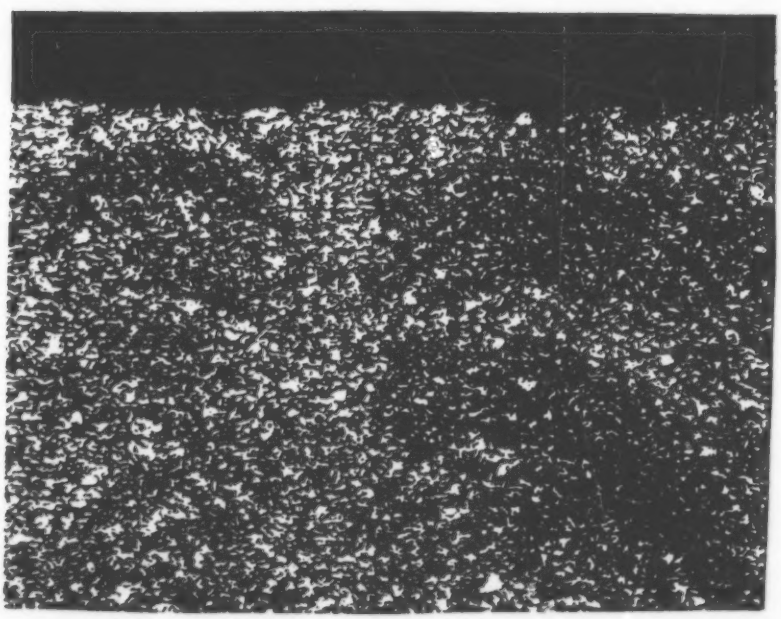

200X Magnification
Etched in 2% Nital

Figure 37

Photograph of Polished Coupon IL15 (Experiment 1)

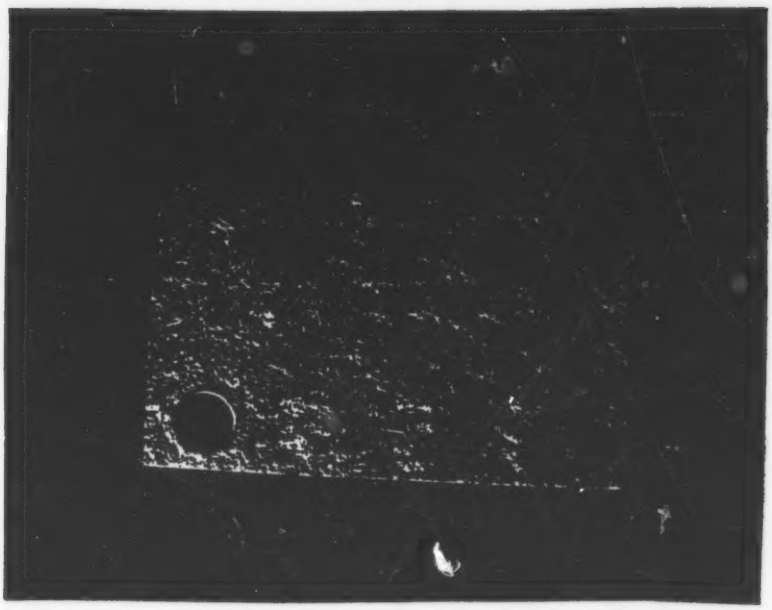

2.7X Magnification
Etched in 2% Nital

10% CO_2, 60% H_2S,
30% N_2, 150°C
Modified Brine

Figure 38

Photomicrograph of Polished Coupon IL15

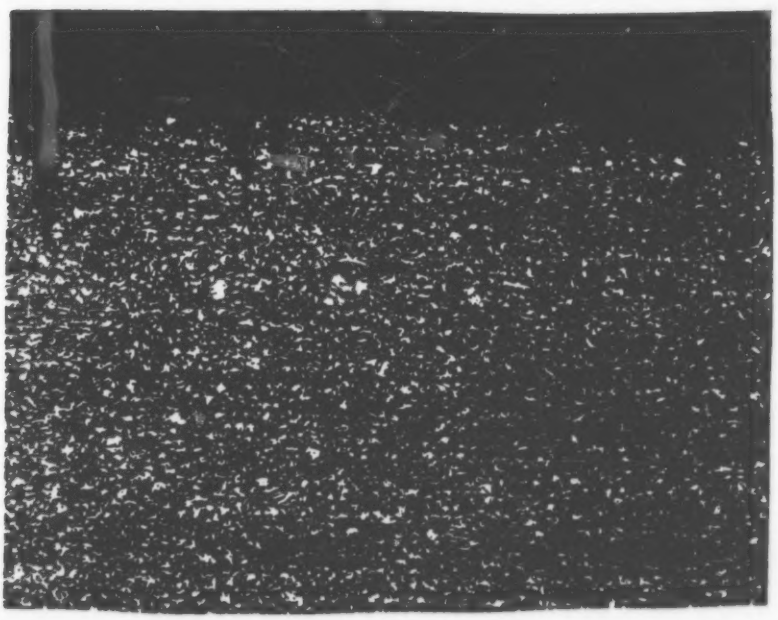

200X Magnification
Etched in 2% Nital

Transverse
Cross-section

Figure 39

Photomicrograph of Polished Coupon IL15 Remote from the Weld

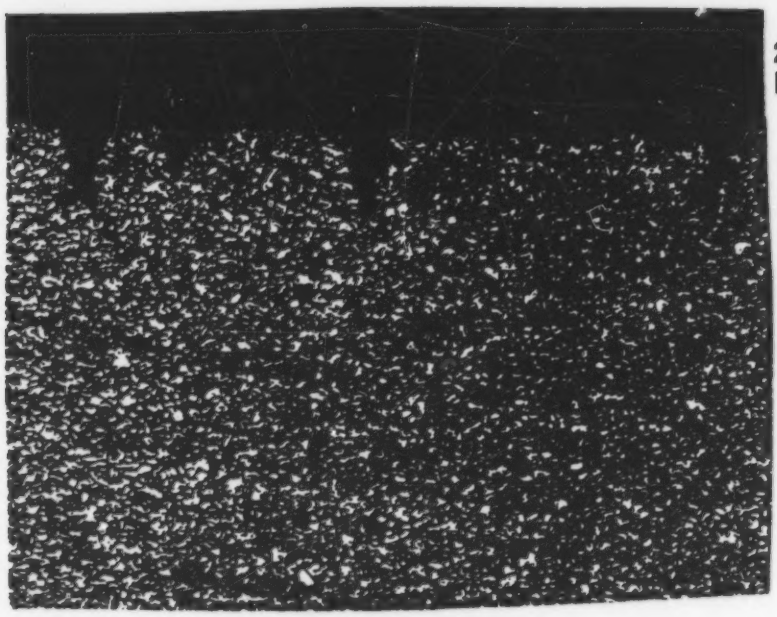

200X Magnification
Etched in 2% Nital

Figure 40

Photomicrograph of Polished Coupon IL15 at the Weld

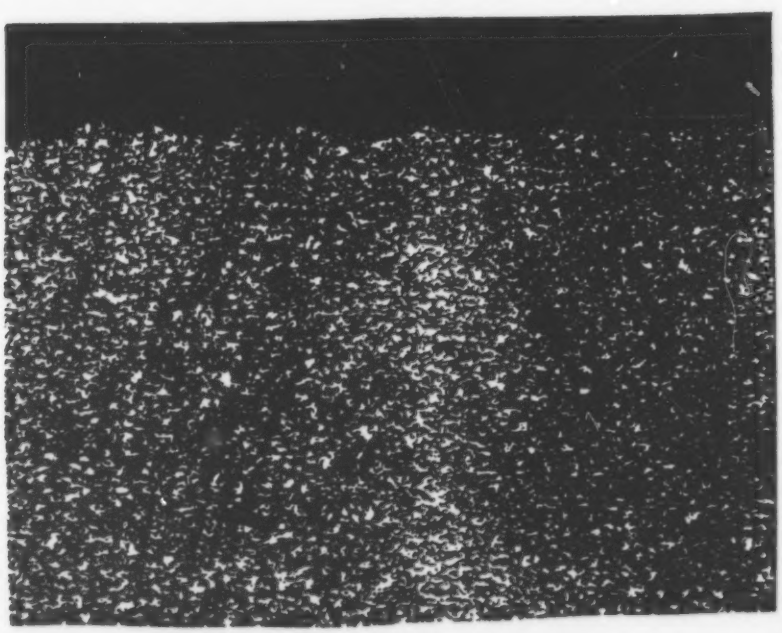

200X Magnification
Etched in 2% Nital